Physics of amniote formation

Vincent Fleury,[1,*] Ameya Vaishnavi Murukutla,[1] Nicolas R. Chevalier,[1] Benjamin Gallois,[1] Marina Capellazzi-Resta,[1] Pierre Picquet,[2] and Alexis Peaucelle[1]

[1]*Laboratoire Matière et Systèmes Complexes, UMR 7057, Université Paris Diderot/CNRS, 10 rue Alice Domont et Léonie Duquet, Paris 75013, France*

[2]*Alligator Bay, 62 route du Mont Saint-Michel, Beauvoir 50170, Manche, France*

(Received 12 February 2016; revised manuscript received 19 July 2016; published 31 August 2016)

We present a detailed study of the formation of the amniotic sac in the avian embryo, and a comparison with the crocodile amniotic sac. We show that the amniotic sac forms at a circular line of stiffness contrast, separating rings of cell domains. Cells align at this boundary, and this in turn orients and concentrates the tension forces. The tissue fold which forms the amniotic sac is locked exactly along this line due to the colocalization of the stiffness contrast and of the tensile force. In addition, the tensile force plays a regenerative role when the amniotic sac is cut. The fold forming the ventral side of the embryo displays the same characteristics. This work shows that amniote embryogenesis consists of a cascade of buckling events taking place at the boundaries between regions of differing mechanical properties. Hence, amniote embryogenesis relies on a simple and robust biomechanical scheme used repeatedly, and selected ancestrally.

DOI: 10.1103/PhysRevE.94.022426

I. INTRODUCTION

It is an important question whether animal morphogenesis consists of a series of stop-and-go genetic instructions mediated by arbitrary biochemical reactions, or whether it is a phenomenon constrained by fundamental physical laws.

Recently, interdisciplinary approaches to embryo development have shown that vertebrate embryogenesis proceeds by using a few simple large-scale physical phenomena, such as dipolar vortex flows at early stages [1–5] and viscoelastic buckling at subsequent stages of development [4,6,7].

Initially, the fertilized oocyte has a round structure, and it cleaves to form a circular mass of a few thousand cells called the *blastula* [8]. Morphogenetic movements begin at this stage. First, there is a vortex flow centered on a saddle point located at the (presumptive) anus which is driven by a peripheral ring of cells [Fig. 1(a)] [4,5]. In the area of the saddle point of this vortex flow, the thin film of cells involutes [Fig. 1(b)] and a capillary wetting called *gastrulation* [3,8] is triggered. By the end of this wetting phase, the blastula is deformed in the anteroposterior direction by cellular pull biased along the elongation direction of the saddle point [Fig. 1(c)]. This pull deforms and folds the tissue in a very specific and reproducible way, by which a bilateral animal is rapidly formed [Fig. 1(d)] [4,9,10].

On analyzing the folding process [4], it is observed that the dorsal side folds along the median axis in a tubular fashion to form the neural tube. The lateral tissue wraps this neural tube in another "tube" identified as the body. Now, in the case of amniotes (reptiles, birds, mammals), the animal is itself wrapped again by a double-sided membrane called the amniotic sac (the internal face of the fold) and the chorion (the external face of the fold). The amniotic sac is commonly referred to as the "bag of waters" [8,11–13]. This is at variance with cephalochordates, fish, and amphibians, which develop directly in their surrounding aqueous medium.

There exist few if any high resolution time lapse imaging examples of amniote morphogenesis, which is generally described in terms of low resolution still pictures corresponding to conventional stages [14]. These do not provide precise dynamic physical information. The biomechanical context, causes, and effects of amniote formation have not been clearly demonstrated, and the exact order of events is not well defined.

A mechanistic understanding of embryo development requires addressing the dynamics of long ranged stress and deformation fields in the tissues. Such a mechanistic approach makes it possible to understand the underpinnings of the evolution of body plans without referring to arbitrary archetypes (as those defined by Darwin [15] or Owen [16][1]).

From a physical point of view, the reference configuration for embryo formation is that of a nonhomogeneous disk. This "blastula" is formed of a regular set of rings (Figs. 2 and 3), somewhat reminiscent of tree rings, albeit very soft. These rings become elongated in the form of "figure eight" rings by the anteroposterior (AP) tissue flow exerted by mesoderm traction along the AP axis, and then fold along the AP direction by buckling. Propagation of the folding wave down to the anus generates the tubes by "rolling up." It has been shown recently that the dorsal folds of the embryo are confined to the boundaries between such encased rings [4]. The folds arise exactly at the boundaries of cell territories because of the difference in their elastic properties which is due to the difference in cell size.

In this article we address the question of whether such a mechanism would be conserved during formation of other folds such as the amniotic sac and the ventral folds. This would

*Corresponding author: vincent.fleury@univ-paris-diderot.fr

[1]Archetype as defined by Darwin: "ideal primitive form upon which all the beings of a group seem to be organized." Archetype as defined by Owen: "that ideal original or fundamental pattern on which a natural group of animals or system of organs has been constructed, and to modifications of which the various forms of such animals or organs may be referred".

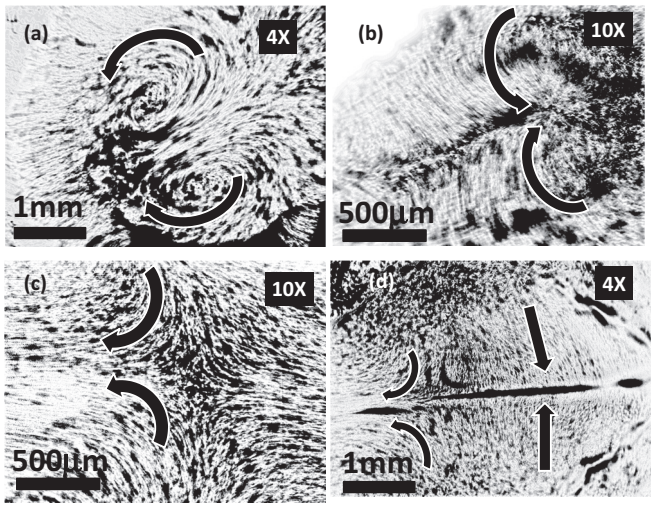

FIG. 1. The initial stages of vertebrate embryo formation are characterized by large-scale movements. First the embryo revolves in a pattern of eddies [(a) top left] [1,2], driven by a peripheral ring of cells. There is a stagnation point in the presumptive anal area. Next, the thin film involutes around the stagnation point of the vortical pattern [(b) top right] [3]. This involution stretches the thin film in the anterior direction along the median axis [(c) bottom left]. This stretch (plus the continuing involution) folds the thin film surface [(d) bottom right] at lines of elasticity contrast [4,9]. These flows are continuous and they create a pattern of folds recognized as a rudimentary bilateral animal. The images of the cell trajectories are obtained by superimposing and thresholding ∼30 min of development taken from time-lapse videos of these movements.

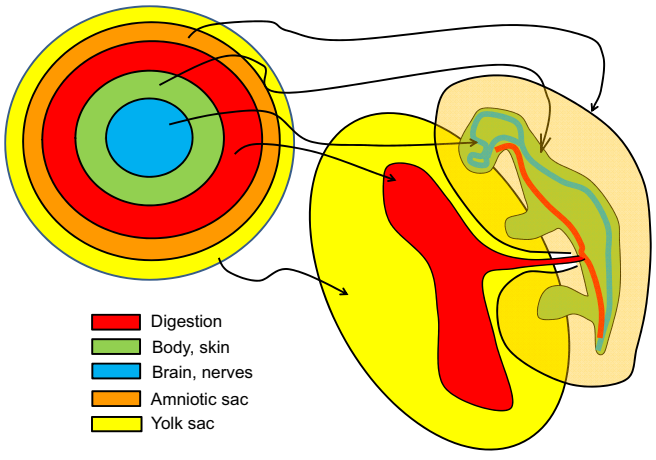

FIG. 2. Principle of construction of the amniote embryo. The blastula is composed of a succession of rings associated to different cells. These cells are characterized by different sizes, and hence by different mechanical properties. During embryogenesis the tissue buckles systematically at the boundaries between cell territories. Each buckling event creates a hollow cylinder (first the neural tube, then the body, then the digestive tube). The peripheral ring forms the amniotic sac. The final topology of the buckled blastula is that of "cylinders inside cylinders, inside cylinders," eventually identified as neural and digestive tubes, inside the body tube, itself inside the chorio-amniotic sac.

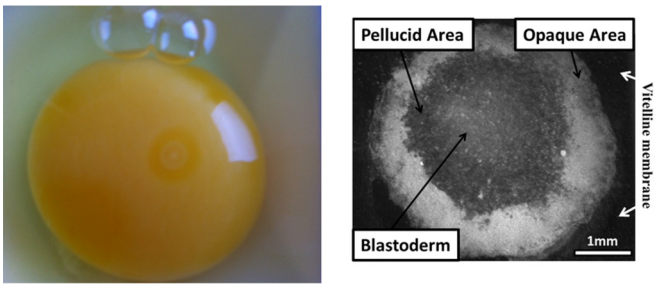

FIG. 3. The "reference configuration" for formation of the avian embryo is a round mass of cells which has an internal structure composed of rings (called a *blastula*). To the left, the low resolution image of an early fertilized chicken egg showing a conspicuous ring structure. To the right, a 4× image of a blastula showing the ring structure of the tissue. The central disk, called a *blastoderm*, will form the embryonic body; the surrounding rings form the extraembryonic organs.

complete a simple scenario of vertebrate morphogenesis, leaning towards the evolutionary aspects.

In the fossil record, amniotes appear about 340 million years (My) ago with the early reptiles [17,18]. It is known that the first event of amnion formation is the appearance of a fold located anterior to the head, which puckers and constricts like a purse string [19,20]. It is also known that an actin cable runs through the cells aligned along the edge of the fold and drives its constriction [21,22]. In Sec. III A we analyze in detail the kinetics of this phenomenon and show that the amniotic fold follows a specific cellular ring. In Sec. III B we show that there exists a contrast of elasticity between this ring and the rest of the tissue. In Sec. III C we show that cells in the territory of the presumptive amniotic sac progressively align themselves to form an ordered belt. Cell alignment propagates from the stiffer ring of the blastula, inwardly. In Sec. III D we show that these alignments are associated to a tension force, and that this tension force itself contributes in return to aligning cells. In Sec. III E we address the formation of the ventral fold. We show that fold generation at domain boundaries also applies to the fold oriented ventrally which forms the body cavity. Together with existing data [4,9,10], this shows that the amniotic fold, the flank folds, and the neural folds follow the same scheme of folding at initially circular lines, where steps of stiffness and anisotropic tension are localized, thereby constituting a fundamental, general, physical mechanism.

In Sec. III F we confirm our results by *in vivo* time lapse in a different taxon which separated from birds about 350 My ago, namely, the Nile crocodile *Crocodylus niloticus*. Since the amniotes appeared about 350 My ago (during the Carboniferous Period [17,18]), and birds separated from dinosaurs about 200 My ago (during the Jurassic Period), it is not obvious that the situation observed in existing birds reflects the evolutionary origin of the amniotic sac. This is why we performed a few experiments with crocodile embryos for confirmation. Crocodiles, or alligators, have become popular in recent years for morphogenetic studies for different reasons. They have been used as a model to demonstrate the role of stress fields in scale pattern formation [23], and also for the study of teeth development and regeneration [24]. Here, we were able to

observe the crocodile embryo during formation and closure of its amniotic sac, including by time lapse. A specific section is dedicated to these experiments which prove that the main features of amniote development, from cell alignment under stress to global pattern formation, are ancestral.

II. MATERIALS AND METHODS

A. Embryos

We worked with chicken embryos at early developmental stages. More specifically, chicken embryos between HH stages 5 and 17 were studied [14]. During that interval of time, the amniotic sac, the tail bud, and the ventral folds form. This corresponds to 36–74 h of development at a stabilized temperature of 37 °C. For the experiments, the embryos were removed from their egg. All the yolk was rinsed away. The vitelline membrane was removed, and the embryos were transferred to a transparent substrate (actually a mass of vitelline gel removed with its vitelline membrane from a fresh egg). The entire procedure is described in Appendix: Materials and Methods. Crocodile embryos were recovered after opening the eggs following the protocol described in the Appendix. For time-lapse imaging, the crocodile embryos were transferred to a similar transparent culture medium.

B. Imaging

All imaging was done with HD monochrome video cameras, Stingray 200, from Allied Vision Technologies. For high resolution images ($4\times$,$10\times$,$20\times$) a Nikon Eclipse microscope was used. For low resolution images, a Leica binocular or an Optem tube was used. To increase the contrasts, the embryos were imaged in shadowgraphic mode as described in the Appendix. Almost all videos presented in this article are available in HD format, with generally a temporal resolution of 10 s.

C. Dynamometry

Forces could be measured in the embryo with custom dynamometers developed in the lab for force measurements in the range 1–100 μN. These are based on deflection cantilevers, either thin pulled glass pipettes, or thin pulled elastomer cantilevers (Rhodorsil), as described in the Appendix.

D. Data analysis

Most data analysis relies on tracking displacements in the embryonic tissue. This is done with the software IMAGEJ (courtesy of Wayne Rasband, NIH), with the TRACKER plug-in (courtesy of Olivier Cardoso and Bérangère Abou).

III. RESULTS

A. Kinematics of amniotic sac formation in chicken

We first describe the formation of the amnion in chicken. At day 2 of development, the presumptive wall of the amnion forms a distinct circular boundary located between the yolk sac (YS) and the embryo, inside the extraembryonic territory called the pellucid area [Fig. 4(a)]. Shadowgraph contrast revealed that the extraembryonic tissue surrounding the embryo at this stage was composed of a thin inner zone with large cells [hereafter called the thinner pellucid area (TPA)],

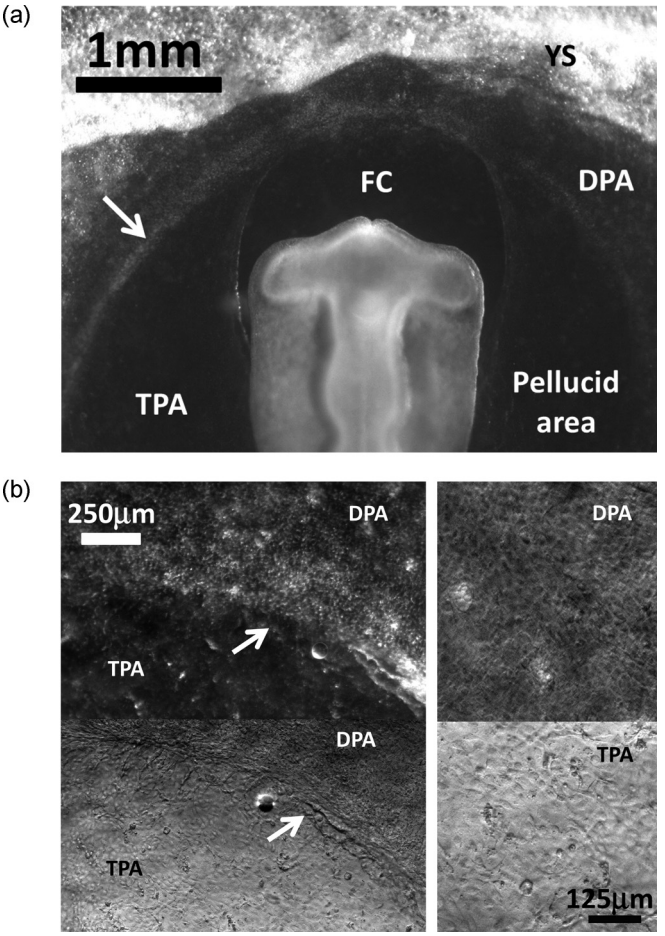

FIG. 4. Embryo morphology during formation of the amnion. (a) At day 2 (HH 12), the presumptive amniotic fold appears merely as a thick shoulder that divides the pellucid area into two morphologically distinct areas: a thin pellucid area (TPA) and a denser pellucid area (DPA). (b) Higher magnification view of the presumptive edge (arrow) of the amniotic fold at HH12 as observed by shadowgraph and grazing illumination microscopy. The TPA (bottom right) features large cells ($\sim$20 μm); cells in the DPA (top right) are smaller ($\sim$16 μm). The cells located at the boundary between TPA and DPA are aligned (bottom left).

and of a thicker outer area [hereafter referred to as the denser pellucid area (DPA)] containing smaller and more densely packed cells [Fig. 4(b)]. The amnion is formed and propagates at the boundary between the thin and the thick zone (see Videos 1 and 2 in the Supplemental Material [25]). The amnion fold forms first in the anterior area, and it moves as a folding wave in the posterior direction. Another folding process occurs in the posterior area beyond the tail region, which generates a fold progressing in the anterior direction (Video 3 [25]). The two folds eventually coalesce to form the amnion (Fig. 5).

The denser ring of cells surrounding the pellucid area was already visible (Fig. 6, top left) at the primitive-streak stage (HH stage 4). In the anterior region, during chord extension (recession of Hensen's node) and up to formation of the first vertebrae precursors ($\sim$4-somites stage), the DPA was stretched and pulled inwards along its inner boundary (TPA-DPA) by the primitive streak (Video 4 [25]). Its outer

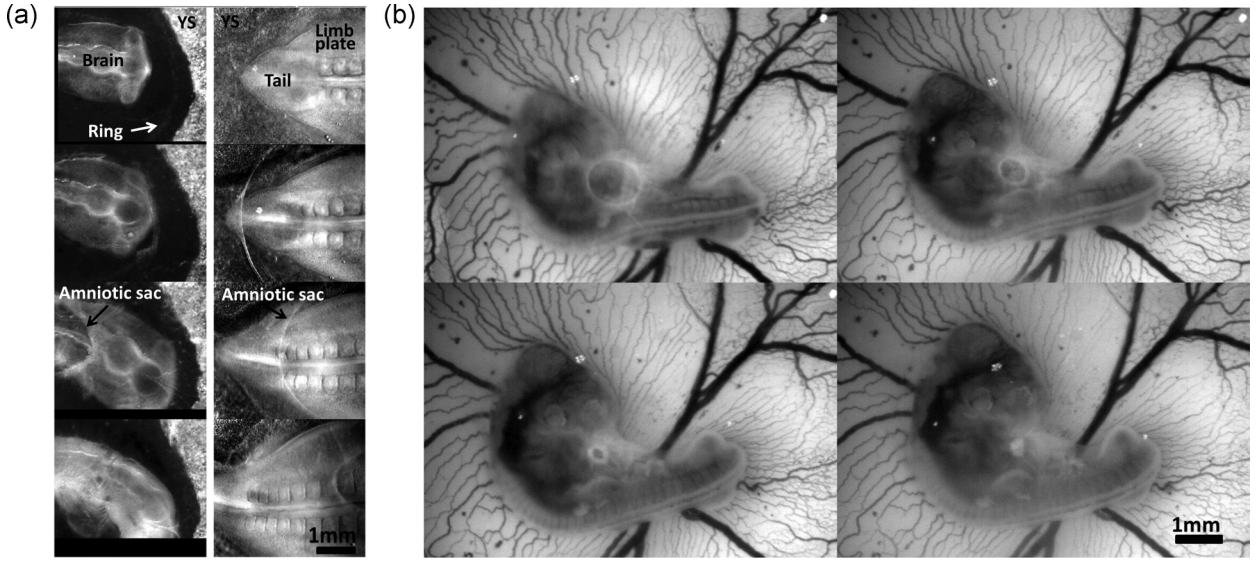

FIG. 5. (a) Formation of the anterior and the posterior edges of the amniotic sac. The anterior edge forms by a pull of the foregut crescent, which pulls upon a circular edge of aligned cells which constricts (left). In the posterior part, the tail bud shears the surface and triggers another contraction wave (right). The folds coalesce to form a circular purse string (b), which closes until there remains only a small scar on the amnion.

boundary (DPA-YS) was pulled radially outwards by the expanding yolk sac.

Time-lapse imaging revealed that the dynamics of amnion formation in the anterior region was divided into two phases. In the first phase, a fold formed which ran along the edge of the foregut crescent (FC) (Fig. 7) (the foregut crescent is a second order division of the blastula rings into sectors; it is not this fold which is going to be forming the amnion). In a second phase simultaneous with the formation and posterior pull of the FC, the anterior boundary between the TPA and the DPA constricted and also folded (Videos 1 and 2). This fold ran along the boundary between the TPA and DPA that was already evident prior to folding and started drawing together like purse strings. The fold of the amnion fold rapidly caught up the fold at the boundary between the FC and the TPA and wrapped it up (see Videos 1 and 2).

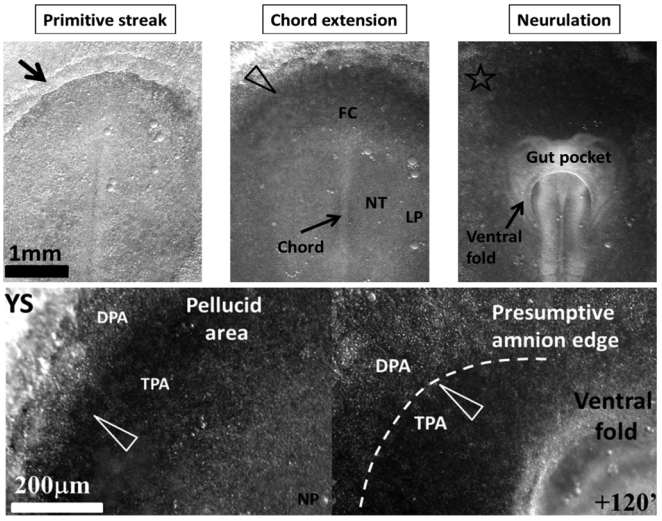

FIG. 6. Origin of the edge of the amnion. Top: Snapshots from a ventral-side time-lapse video at primitive-streak, chord-extension, and neurulation stages (same embryo, from Video 4). A dense ring of cells is already visible at the periphery of the pellucid area at the primitive-streak stage (top left, arrow). At the chord-extension stage, the dense ring is pulled and stretched in the posterior direction (top middle, arrowhead). The boundary between DPA and TPA appears during neurulation as a layer of cells that progresses inward (top right, star). Bottom: Higher magnification in the anterior area shows the retrograde progression of the cell layer and of the foregut crescent as the embryo starts to neurulate (snapshots separated by 2 h, from Video 4). NT: neural territory; FC: foregut crescent; TPA: thinner pellucid area; DPA: dense pellucid area; YS: yolk sac; LP: lateral plate.

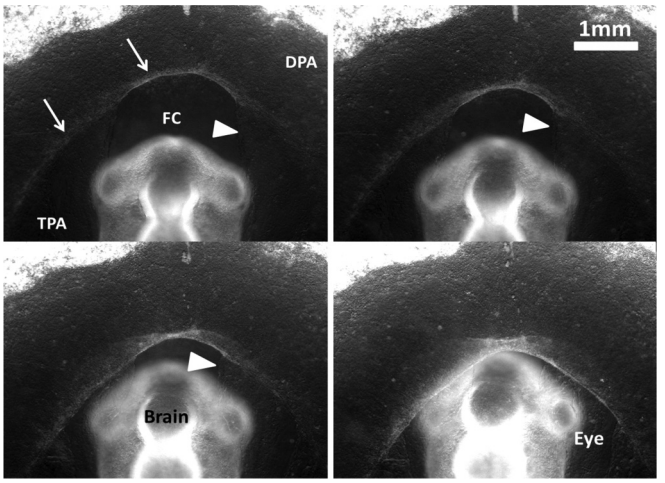

FIG. 7. Dynamics of amnion formation (see Videos 1 and 2). The formation of the amniotic fold (transmission light in grazing illumination) consists of two phases. In a preliminary phase a fold forms which parallels the body of the animal (arrowhead). This fold follows the boundary of the foregut crescent (FC). In a second phase, the boundary between the dense pellucid area (DPA) and the thin pellucid area (TPA) buckles over the fold of the FC and wraps the body by contracting like the string of a purse. The amniotic fold strictly follows the boundary between TPA and DPA (arrows).

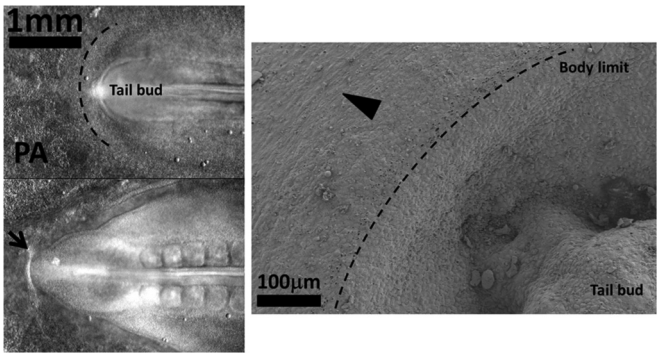

FIG. 8. Triggering of the posterior fold. When the formation of the amniotic sac is followed dynamically and with a higher resolution it is observed that the tail bud passes over the boundary of the blastoderm (presumptive body limit), and shears the surface (arrow) of the pellucid area (PA); this shear triggers a contraction wave which forms the amnios (Video 3). The fold buckled by the tail bud is not exactly the one which forms the edge of the amnion. The edge of the fold is formed by the ring of cells which constricts actively after being triggered. We performed SEM analysis on fixed embryos at a stage identical to the first plate in Video 3, to confirm that the ring of aligned cells is located very close to the area sheared by the tail bud, somewhat away from the presumptive body limit, in the centrifugal direction (arrowhead in the SEM image).

In the posterior area the situation is different: The ring of cells forming the presumptive amnion fold is located much closer to the embryo body. Because of the initial asymmetry of gastrulation and of the extension of the embryo axis, the embryo territory extends more in the posterior direction than in the anterior one (see Fig. 1). We observed that the apex of the tail bud stresses the pellucid surface as it grows (Video 3). Scanning electron microscopy (SEM) imaging of an embryo at almost the same stage as Video 3 confirms that the area which is stressed by the tail bud in Video 3 corresponds to the ring of aligned cells which surrounds the embryonic territory (Fig. 8, right). The contact of the tail bud with the surface triggers the folding event, which rapidly wraps the posterior part of the chicken body (Fig. 8, from Video 3), until a bag is completed by coalescence with the anterior fold. Please note that the posterior amniotic fold in Video 3 is not the little fold formed by the tail bud which is visible in Fig. 8, right. We confirmed this in a second time lapse (Video 5 [25]). A detailed observation of Video 5 shows that the tail bud shears and buckles the surface of the tissue surrounding the embryo, but the amniotic fold is triggered slightly away from this physical fold, towards the posterior direction; the same situation is seen in Video 3. This demonstrates the fact that the initial position and the subsequent dynamics of the amniotic fold is intrinsic to the presumptive amniotic territory, and that the amniotic fold is merely triggered by the growth of the tail bud.

B. Elasticity of the territories on either side of the presumptive amnion

We next measured the deformations of the DPA and of the TPA in the anterior area when the embryos were mechanically stretched or compressed along the anteroposterior axis (Video 6 [25]), prior to the formation of the amniotic sac. We found that the DPA had a greater (close to a factor of 2) tensile stiffness than the TPA [Fig. 9(a)]. We also measured the applied force (see the Appendix). Similar stretch and compression experiments were performed along the median axis in the posterior area at a stage when the tail bud was still in plane with the pellucid area. We show in Video 7 [25] a uniaxial traction and compression test of this area, whose analysis is displayed in Fig. 9(b). By particle imaging velocimetry (PIV) analysis of the deformations along the median axis we found again an elastic contrast between territories [Fig. 9(b)], with the stiffer tissue being the tail bud. The anal area in series with the tail bud is less stiff; the limb tissue has even lower stiffness. Around the embryo, one finds the soft extraembryonic tissue, and around this soft tissue, one finds a stiff belt corresponding to the amnion territory [Fig. 9(b)]. Therefore, the tail bud behaves as a stiff rod pushing the softer surrounding tissue, and the thin pellucid area is the softer area located in between two stiffer areas, the embryo itself and the denser pellucid area.

Now, could the buckling of the amnion be the result of a physical process? To elucidate this question, we worked with 6-somites-stage embryos, prior to amnion formation (which occurs between the 10- and 12-somites stage). We isolated the embryos and relieved the tension exerted by the vitelline membrane by removing the embryos from it. A few minutes after the vitelline membrane was removed, the pellucid area spontaneously pulled together, buckled, and started to wrap itself up around and over the head of the embryo **[**Video 8 [25], Fig. 9(c)**]**. This rapid, mechanically induced buckling took place along the line separating the DPA and TPA, as early as 10 h before the physiological *in vivo* transformation took place. This proves that the mechanical landscape in the extraembryonic territory is prepatterned, and that the magnitude of stresses at the DPA-TPA boundary is in the proper range for buckling. The respective orientations of the fold and of the head guaranteed that the fold slipped *over* the head of the embryo, thus wrapping it up, rather than slipping under it (which would be catastrophic as it would get stalled against the gut pocket as well as the heart of the embryo). We next fastened micromechanical tools to the embryos to actively stretch and compress them either along the anteroposterior axis, or along a direction slightly tilted away from anteroposterior axis **[**Video 9 [25], Fig. 9(d)**]**. In all cases, the pellucid area systematically buckled along the same boundary. A similar result in the posterior area is evidenced in Video 7. Quantitative analysis shows that the buckling occurs on the soft side of the pellucid area, along the stiffer side [Fig. 9(b), bottom right; from Video 7]. When we overlap the data plot showing the tissue stiffness (gradient of the displacement) over the image at the instant of buckling, we see that buckling occurs exactly on the soft area along the stiff belt. It should be noted with attention that the film in Video 7 corresponds to an embryo at exactly the same stage as the SEM picture in Fig. 8. The fold which is formed during the compression test during the buckling event is indeed quite close to the belt of aligned cells.

This shows that the location of the fold is so strongly prepatterned all around the embryo, by its mechanical properties, that it is not sensitive to the detail of the mechanical stress that triggers the buckling event. The contrast of elasticity provides the mechanical prepatterning: Buckling systematically occurs along the line that separates regions of differing elasticity.

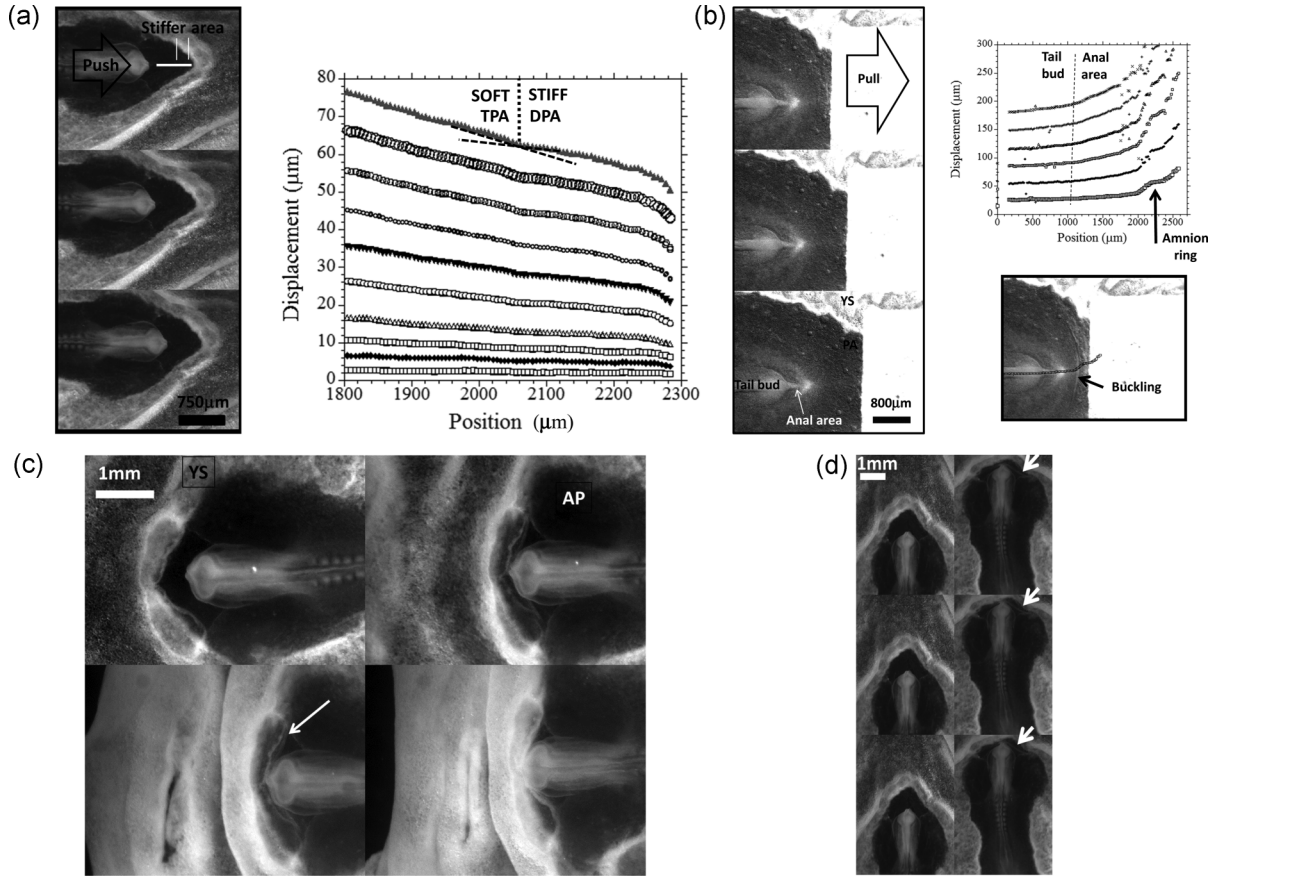

FIG. 9. (a) Gradient of elastic properties between the presumptive amnion and the rest of the pellucid area in the anterior area. Small metallic rakes controlled via a micromanipulator are used to stretch or compress the embryo; the applied force is measured by an elastomer as described in Ref. [4]. Left: A typical compression experiment (from Video 6). Right: PIV displacement measurement along a line crossing the pellucid area, for increasing compression. The deformation is defined as the derivative of the displacement (slope of the curve). The TPA is approximately twice as soft as the DPA: the discontinuity of the slopes of the displacement occurs exactly at the position where the pellucid area starts to fold (see the end of Video 6). (b) Uniaxial stretch and compression in the posterior area (from Video 7, during the compression, buckling of the surface occurs). The stretch test shows that there is a soft ring surrounding the embryonic territory, followed by a rigid belt corresponding to the amniotic tissue. When the test bench is used in compressive mode (bottom left) it is observed that the surface buckles in a prepatterned area; we overlap the displacement curve on the configuration at the moment of buckling: This clearly shows that the buckling event is localized on the softer side of the tissue surrounding the embryo, the stiffer part behaving as an undeformable element compressing the soft tissue. (c) Formation of the amniotic fold by anticipation. When an embryo is detached from the vitelline membrane while the amniotic fold is not yet formed, and the embryo is allowed to relax the stress on its own in a Petri dish (for example, here at the 6-somites stage), one observes a rapid constriction of the entire embryo (by the minute) and a sudden spontaneous buckling of the tissue in the anterior area, where a fold forms, which even passes over the embryonic head (see Video 8). This means that the tissue is prepatterned to form a fold long before the fold actually forms, and that the forward curvature of the embryo implies "automatically" that the fold passes over the head. At these stages, the amnion formation is retarded in the physiological case, by the circumferential stretch along the perimeter of the yolk sac which, by stretching centrifugally the entire tissue, hinders the movement shown in Video 8. It also shows that the internal stresses are in the proper regime for buckling. YS = yolk sac; AP = area pellucida. (d) Amnion buckling with micromechanical tools. An embryo is detached from the vitelline membrane at a stage when the amniotic fold is not yet formed (here the 6-somites stage). It is grasped with metallic rakes and stretched back and forth along the anteroposterior axis (see Video 9). It is observed that the anterior area buckles systematically along the same line corresponding to the position of the amniotic fold (arrow). This means that the mechanical properties prepattern the tissue, and that the folding event which generates the amnion is not quite sensitive to the detail of the force pattern.

C. Cells are aligned along the presumptive amnion edge

Using shadowgraph contrast imaging, we tracked the DPA-TPA edge (Videos 2 and 10–14) 6 h before folding (7-somites stage, Fig. 10, from Videos 10 and 11 [25]), and at the point in time when folding occurred (Figs. 11 and 12 from Videos 2, 12, and 13 [25]). We observed that cells in the soft area were being dynamically aligned along the TPA-DPA boundary to form a belt of aligned cells $\sim$150 μm wide on the DPA side [Fig. 10, box 10×; see also Video 11 at magnification (Mag.) 20×]. This alignment became increasingly marked (from side to middle), as the moment of amnion folding approached (Videos 2 and 12). The boundary constriction progressively became an edge: Video 12 shows a high spatial and temporal resolution of the exact moment of folding (Mag. 10×). (Video 2 shows a 4× Mag.). This constriction stretched along the entire tissue in the DPA, perpendicularly to the closing "purse string" (i.e.,

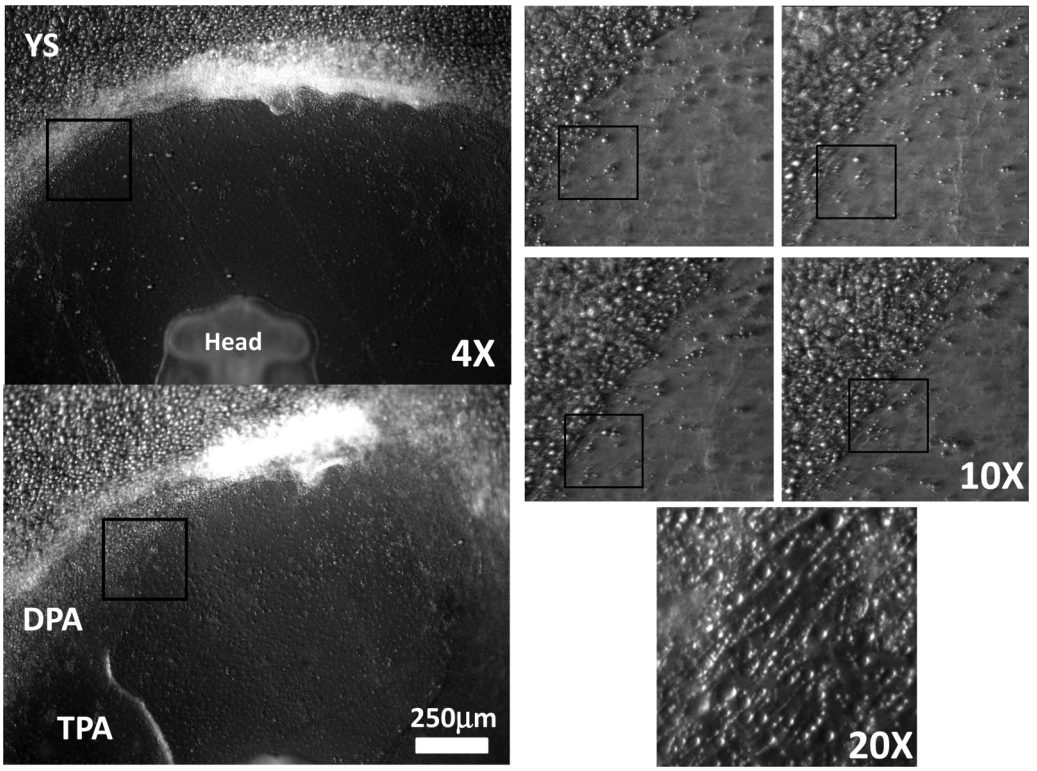

FIG. 10. Formation of the belt of aligned cells. Starting at the 5-somites stage, the belt of aligned cells progressively widens and exerts a traction force to generate the amnion. The cells are imaged from the ventral side; the embryo is incubated upside down. Left: pellucid area, ahead of the embryo, at two time intervals separated by 6 h (Mag. 4×). The belt of aligned cells widens (box). Right: Higher magnification (Mag. 10×) and time-lapse imaging (Video 10) reveal that cells on the internal side of the pellucid area are recruited and align themselves along the already aligned cells (boxes). The area of aligned cells widens at the expense of the softer cells (duration of the video is 5 h). The Mag. 20× shows the alignment of cells at a cell-resolved scale (Video 11); Video 11 shows the very active cellular traffic in that area (duration of Video 11 is 40 min) caused by softer cells moving tangentially to the stiffer ring of the yolk sac (YS: yolk sac; DPA: dense pellucid area; TPA: thin pellucid area).

radially, centripetally) and formed a sac [Fig. 11(a)]. Cells were oriented radially at the core of the DPA but orthoradially at the DPA-TPA border; the very dynamic differences of orientation are particularly visible in Video 14 [25].

We performed SEM imaging of fixed chicken amniotic sacs, which confirmed that the cells are aligned along the edge of the fold where the cells are stretched orthoradially, but tend to be oriented perpendicularly away from the edge, where the tissue is stretched radially [Fig. 13(a)]. The SEM images also enabled us to measure the thickness of the amnion at this stage [Fig. 13(b), thickness 10–20 μm]. It has a two-cell thickness.

We analyzed the deformation (especially shear) at the exact moment when the edge of the amniotic sac forms in chicken [Fig. 12(b)]. At this moment, the tissue bifurcates from a planar surface to a sigmoid surface with an overhang. We observed that the shear was oriented circumferentially [Fig. 12(b) along the TPA-DPA border (on the TPA side)], suggesting that the edge is subject to mechanical tension.

D. Tension induces cell alignments in the amnion

In order to prove the existence of mechanical tension, we cut the edge of the ring with small dissection scissors. The two halves of the tissue on either side of the cut rapidly separated, forming a wedge, thereby confirming the presence of mechanical tension in the edge (see Video 15 [25] and Fig. 14(a), top left). For cuts going beyond the belt of aligned cells, the opening angle of the cut was greatest at the edge and radically reduced further on into the tissue [Fig. 14(b)]. Thus we see that the tensile force is localized along the boundary, in the narrow belt where cells are aligned: There is a surface tension gradient close to the boundary between the two cell domains. After the incision, the tensile force could no longer be transmitted through the cut. A new bundle of aligned cells aggregated along the cut, forming a new edge [Figs. 14(a) and 15], and the amnion resumed a normal constriction process, with a regenerated ridge (Video 16 [25]). Surprisingly, even large wounds healed [Fig. 15(a), left)]. It took no longer than 10 min after a cut like the one shown in Video 15 for the tissue to regenerate an actively constricting edge by realignment of the cells around the cut [Video 17 [25], and Fig. 15(a), right]. The incision test shows that tensile stress can induce cell alignments in the force range exerted by the ring of cells along the edge. The cells around the wound react by realigning and generating a feedback constriction running opposite to that of the tensile force, ending in resumption of the closure process and regeneration of a purse string (Videos 16 and 17).

For deep cuts (three cases out of ten), the mismatch between the tensile stress patterns before and after the cut led to the formation of a completely new edge that ran parallel to the

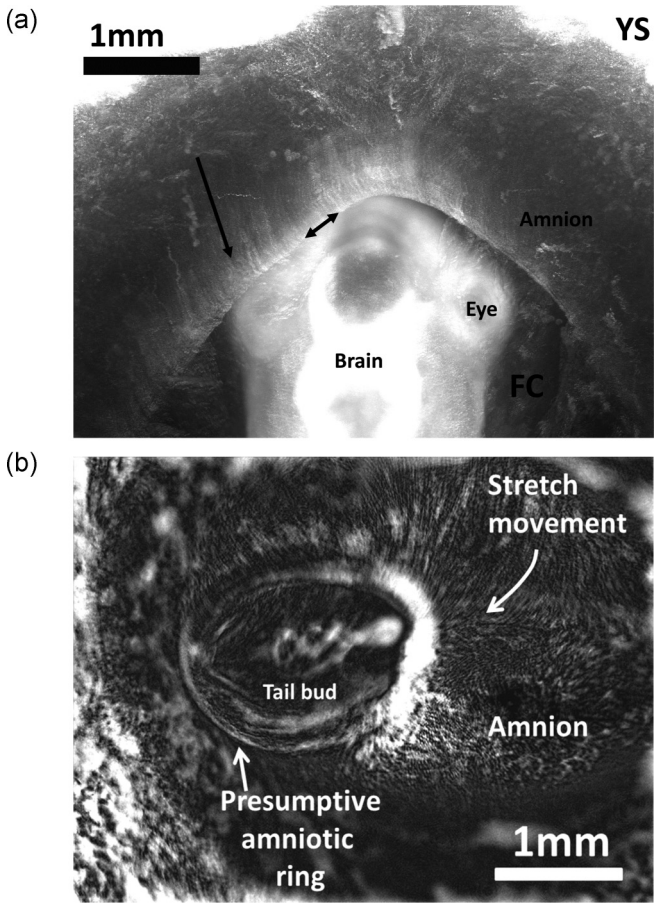

FIG. 11. (a) *Z*-stack projection (IMAGEJ software) during closure of the amniotic bag (chicken embryo). It consists of a radial pull in the tissue (arrow) and an orthoradial constriction along the belt (from Video 13). (b) *Z*-stack projection during closure of the amniotic bag in crocodile.

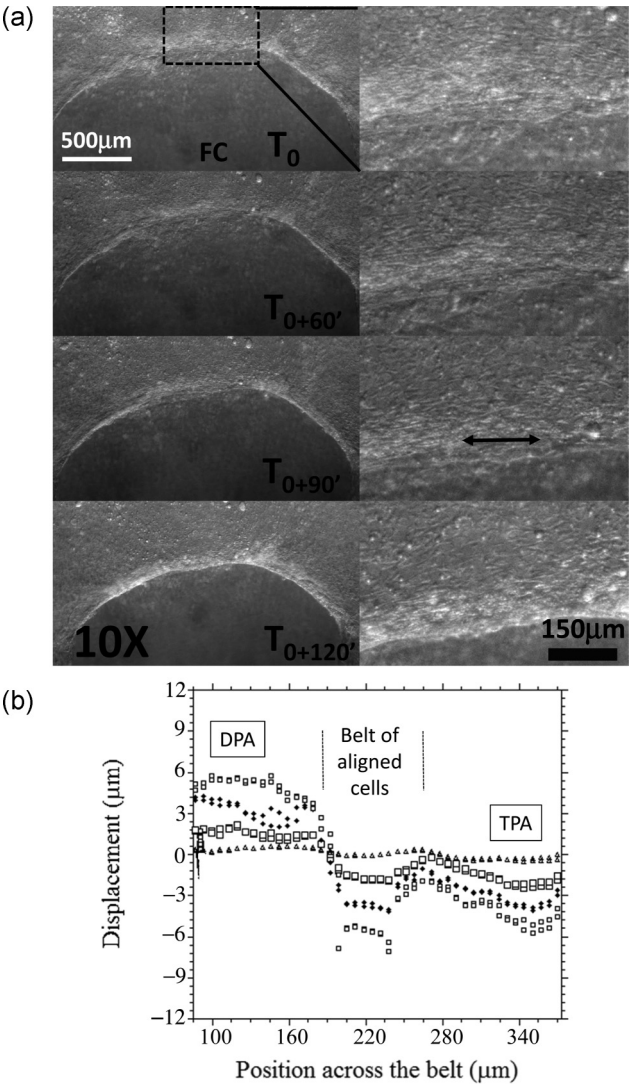

FIG. 12. (a) Cell alignments at the moment of folding. Cells align in a narrow "belt" close to the DPA-TPA boundary (from Video 12). The tensile force generated by these cells makes the amnion fold precisely along this belt. The snapshots show the exact moment of folding of the edge. In the top "T_0," the tissue is 2D; in the "$T_0 + 120$" snapshot, the tissue has buckled in 3D and has a sigmoid shape. The tensile force also recruits cells laterally as the fold wave progresses (Video 14). Supracellular fiber bundles are seen to align along the fold. (b) The shear rate close to the contracting ring is measured (from Video 12, with the same data, albeit a more resolved video file in time and space) by PIV tracking of a line of points normal to the DPA-TPA boundary, prior to the moment of folding, in the region of the double-headed arrow in (a). We measure the longitudinal (orthoradial) displacement of the tissue at 20, 50, 100, and 150 s. The displacement is greater in the belt of cells and exhibits a sharp gradient at the frontiers of the belt (shear rate, 0.24/min).

previous one (see Video 16, at the end). This outstanding regenerative capability proves that all cells in the DPA are able to form a constricting ring as long as they are subject to tensile force. It was observed that misalignment defects ("disclinations") would naturally be wiped out by the tension, as the amnion closure proceeds. It was also observed that in the final stages of closure, radial wrinkles appear on the amnion around the closing hole, obviously as a consequence of radial tensile stress in the amnion [Fig. 15(b)].

We performed simple desktop experiments with rubber sheets, which corroborated the physical generic properties of self-organization in the amnion (Fig. 16). In a first experiment [Fig. 16(a)], we cut a stretched rubber sheet. We observe that the "wound" opens in a pattern identical to the one observed *in vivo*. We also observe that a new buckling event happens and generates instantaneously a new fold bypassing the cut. This is explained by the fact that, if the tissue is stretched with a stress close to the buckling threshold, then, when the edge is cut, the stress increases at the wound boundary, by the amount of stress relieved at the cut and transferred at the edge of the wound. Therefore, it is natural that wounding a fold, caused by buckling, induces spontaneously a new fold, bypassing the wound. In a second simple experiment we prepared a rubber sheet with a misalignment of folds, and progressively pulled on it. We observed that the misaligned ends of the fold bifurcated nonlinearly and were eliminated, just as observed *in vivo* (Fig. 16(b), Video 18 [25]).

In order to measure the tensile force in the edge of the amniotic sac during closure, we pulled it with a thin glass

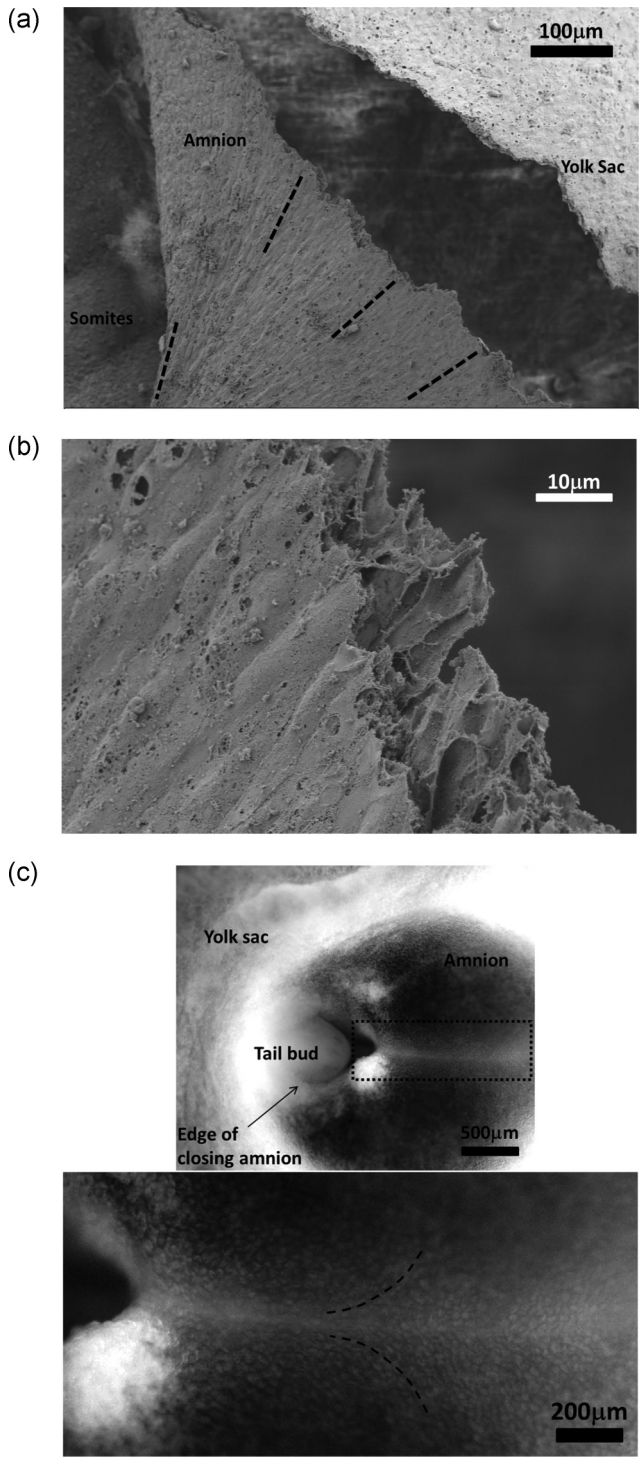

FIG. 13. (a) SEM picture of the edge of the amniotic sac. The image shows the cell alignments which tend to be orthoradial (i.e., tangent) to the ring at the edge of the amniotic circle, and oriented perpendicularly to it (i.e., radially) far away. (b) SEM picture of the cross section of the amniotic sac showing that it is two cell layers thick with a thickness $\sim 10\,\mu$m. (c) *In vivo* image of the closing crocodile amnion showing the stream of cells being aligned in the stretch direction (dashed line).

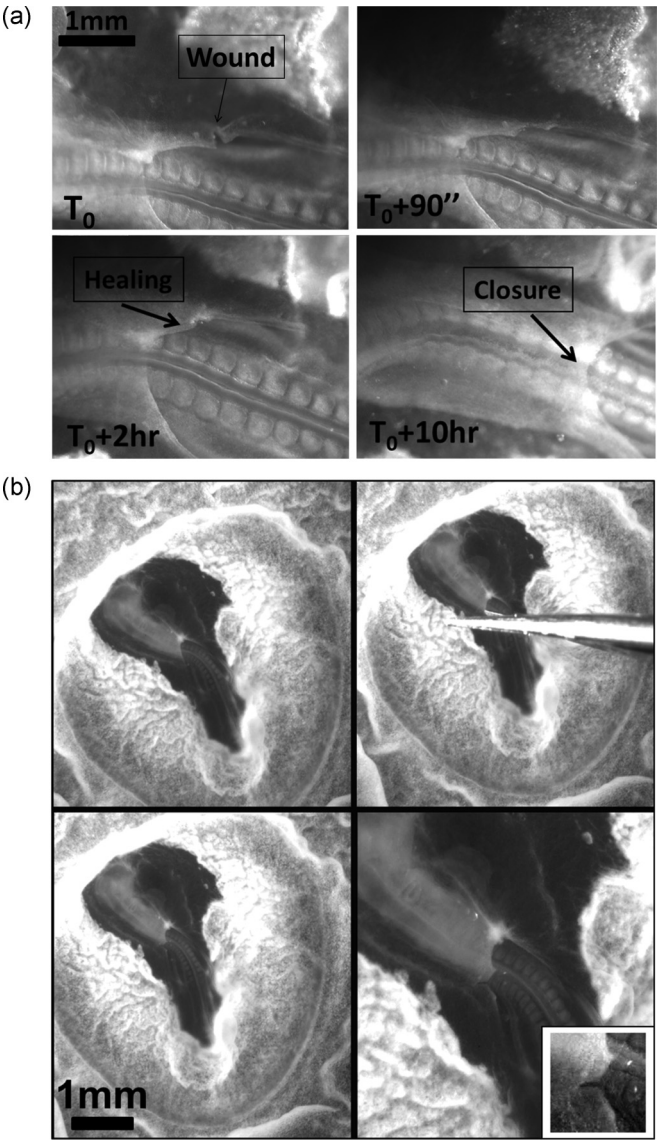

FIG. 14. (a) Wound healing in the amniotic sac. The lips of the wound open rapidly after the cut (Video 15). Remarkably, the wound heals and the edge of the amnion resumes constriction normally (Video 16). If, after the cut was performed, there is a mismatch between the new stretch direction and the existing edge of the amnion, a new buckling event forms an entirely new edge (see end of Video 16). (b) Opening of a wound in the amnion edge. The embryo is removed from the egg and spread flat in a Petri dish. The edge of the amnion is cut with very fine scissors. The wound opens within a few seconds. The form of the wound shows that forces are concentrated along a narrow stripe along the edge of the circle. The bottom right inset shows the wound shortly (<10 s) after the cut. The form of the wedge shows that the tension is larger close to the edge (larger aperture), where there is a belt of parallel cells (see text).

cantilever until we formed a wedge (Fig. 17, top, and Video 19 [25]). In this situation, mechanical equilibrium of the tip of the wedge resulted from a balance between the tension of the edge and the force exerted by the cantilever. Just after having pulled the amnion with the cantilever, the tissue gradually dissipated the applied stress, eventually reaching a tension set point (Fig. 17, bottom). We measured a tension in the amniotic belt of $\sim 10^{-6}$ N. Considering cell sizes and the width of the belt (about 20 cells, counted directly on SEM images), with

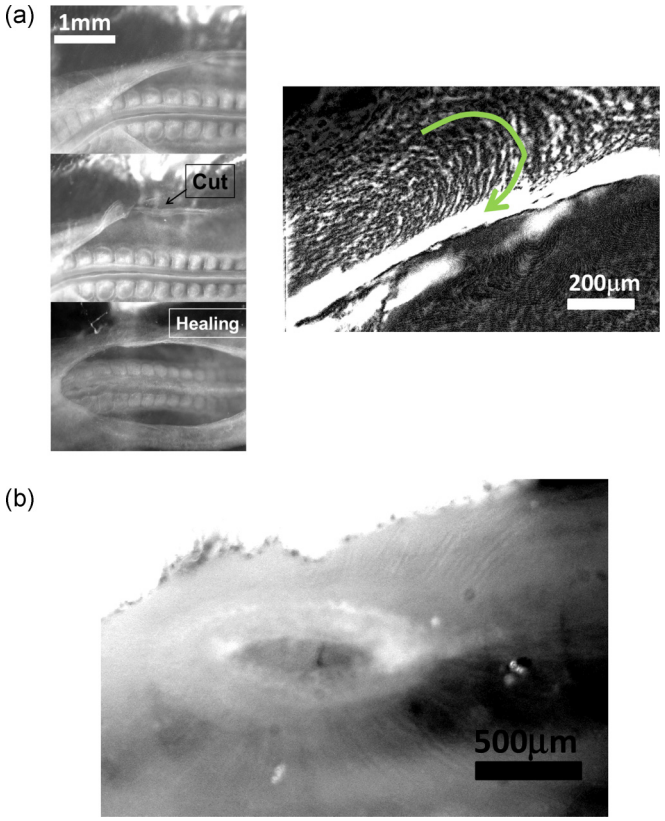

FIG. 15. Surprisingly large wounds in the amnion spontaneously heal under the effect of the localized tension, as shown in this experiment. The plate (left) shows three stages of the "amnion wound" experiment. The top image shows the normal amnion edge while it is progressing towards the right. After the cut, a large wound is formed deep into the amnion surface which hangs like a flag (middle plate). The ten samples examined yielded the same result. Progressively, the edge of the wound is stretched, then it reconstricts and a perfectly regular amnion edge reforms (bottom). To the right, a magnified view of the edge of the amnion during the healing of the wound (same embryo). As the tissue is stretched, cells wind and realign in the tension (time lapse visible in Video 17), until a bundle is reformed. The image to the right actually shows a Z projection of the frames, revealing the winding trajectories of the cells which realign tangentially to the edge of the wound.

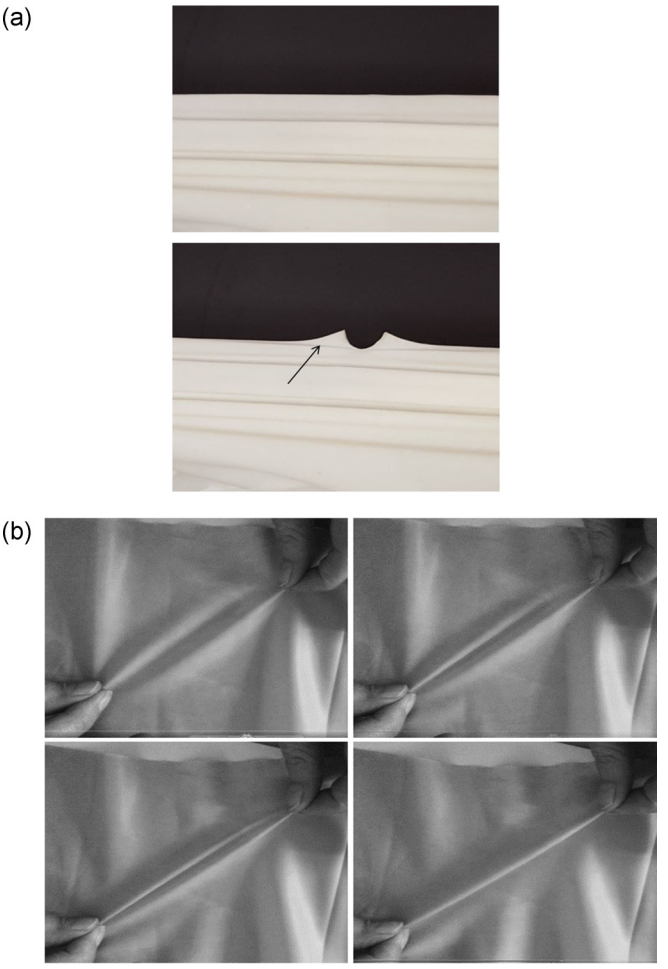

FIG. 16. Elastic analogs. In (a), a rubber foil is stretched up to buckling. It is next wounded along the edge. The contour of the wound along the edge is identical to the one observed *in vivo*. In addition, a new buckling event bypasses the wound. In (b), two folds which are misaligned are stretched. The folds coalesce and form a single straight fold (Video 18). This phenomenon is observed along the amniotic fold (see, for example, Videos 3 and 5).

cells forming a ring about 1000 cells in diameter, a crude estimate of the force per cell yields $\sim 10^{-10}$ N.

Interestingly, during the traction experiment, we observed oscillations of the force as it decreased to reach the final set point. Such oscillations and spikes are also directly visible in the optical view of the embryo during physiological closure of the amniotic sac, and the pattern can be extracted by PIV, from the movies at 10 s temporal resolution. Careful direct analysis of the movies showed that the amniotic territory is actually prone to contractions (Video 2; see also Video 20 [25]). Away from the amniotic purse string, focal, isolated contractions can be observed, which reveal clearly the relaxation behavior of the contractions. These spike to $\sim$10% deformation in less than 1 min, and then relax with a time constant of the order of 3–5 min. Figure 18(a) shows a focal spike (actually in the crocodile amnion). The spikes' morphology can be focal, but closer to the peripheral tissue of the embryo forming the rings of cells which will fold, the spikes are obviously anisotropic [Fig. 18(b)], their pattern following the ring structure [Fig. 18(b) shows a contraction along the ventral ring prior to folding]. This shows that the cell pattern (or cell texture) influences the contraction pattern: Rings of cells generate centripetal contractions. When the behavior of the presumptive amniotic territory of chicken is followed *prior* to formation of the amniotic purse string, as in Video 2, it is observed that the ring of cells constricts (deformation from 1 down to 0.5) with multiple spikes of contraction of the period $\sim$3 min; therefore the contraction pattern prior to formation of the amnion is not monotonic.

E. Similarities of ventral fold formation

We also analyzed the contraction that defines the ventral fold of the body. This contraction occurs in the anterior and in the posterior areas; it forms analogous rings and purse strings, and these coalesce around the navel area to close the ventral

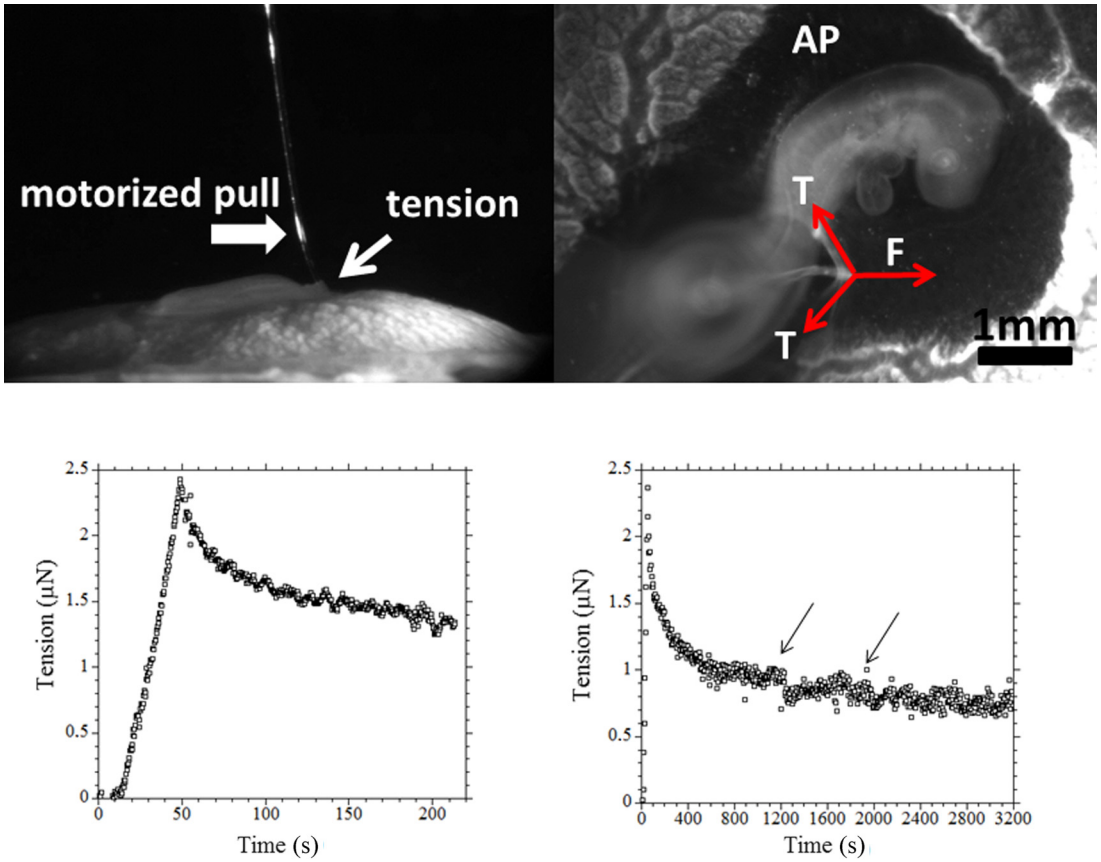

FIG. 17. Measurement of the tension at the edge of the amniotic sac. A thin glass cantilever is moved against the edge of the amnion (top images, lateral and vertical view), with a motorized precision stage, following the method described in Ref. [38] (Video 19). After this initial stretch, the tissue gradually dissipates the stress: Following the flexure angle of the tip of the glass cantilever (bottom, approximately first 4 min and first hour) allows us to compute the value of the tension at the edge as a function of time. The tension at the edge relaxes to an asymptotic set-point value of $\sim 1\ \mu$N (eight samples).

side of the animal. Video 4 [25] shows the contraction of the (flat) ring-shaped tissue located in the anterior area and also associated to head formation, dorsally, and to heart and gut formation ventrally. It rapidly becomes a contracting purse string. A similar contraction is observed at the opposite end in the posterior area around the presumptive limb and hindgut territory (for example, in Video 3). Figure 19 shows the pattern of streamlines, as obtained by superimposing 30 min of these contractions, in the anterior and in the posterior areas (anterior area is observed ventrally; posterior area is observed dorsally in these plates). Please note that the events do not occur at the same time. The contraction in the head area occurs during the early stretch triggering the formation of the neural tube, while the contraction in the posterior area occurs later, when the neural folds are closed, and the tail bud touches that area. The pattern of streamlines [Figs. 19(a) and 19(b)] reveals a localized contraction of the tissue which buckles inwardly. At the anterior side, the ventral fold propagates along the boundary between the lateral plate and the foregut crescent [4,9]. The lateral plate and the foregut crescent are both ring-shaped domains; the lateral plate is encased in the foregut crescent. Cells in the foregut crescent are on average larger than in the lateral plate [4]. In the posterior area, the fold follows the ring-shaped territory forming the boundary of the embryo.

As the anterior ventral fold advanced, the purse string contributed to the formation of the normal heart by bending and twisting the left and right ventricles (Fig. 20(a), Video 21 [25]).

We observed that the boundary between the lateral plate and the foregut crescent constricted posteriorly and recruited cells as it progressed, just like the amnion ring. (The forward dorsal-to-ventral bending of the head and the similar backward bending of the tail are also likely a consequence of the tissue being pulled by the ventral purse strings).

Performing the wounding experiment described above for the amnion, along the midline of the ventral fold, resulted in a rapid opening at the site of the wound analogous to the one observed in the amnion wounding experiment, showing that the ventral fold is also under mechanical tension at the edge of the purse string (Video 22 [25]).

When the cut was performed after the 6-somites stage, the wound healed and resumed normal constriction (Video 23 [25]). The heart ventricles were, however, not bent or looped as observed physiologically [Fig. 20(b)], due to the delay in morphogenesis induced by the wound. When the cut was performed earlier, between the 3- and 5-somites stage, the tension made the tissue around the site of the cut creep apart; heart territories were not pulled together at all, nor twisted properly by the purse-string effect (Video 24 [25]). In this case the presumptive heart territories formed two well separated, independently beating ventricles (Figs. 20(c) and

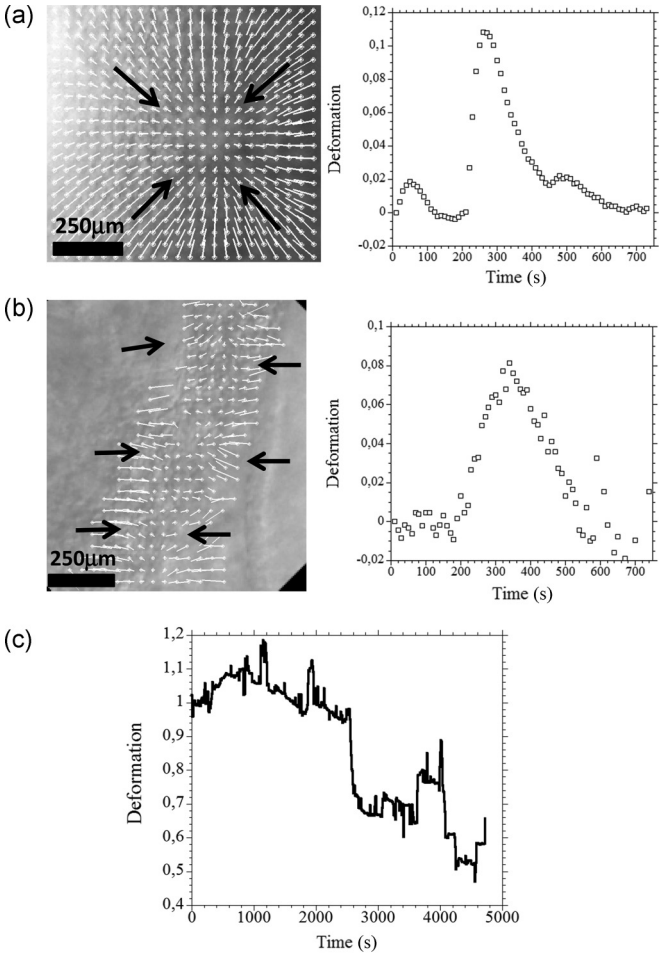

FIG. 18. Oscillatory behavior of the tension forces in the embryonic tissue The oscillations observed in the amnion can be focal (a central pacemaker provokes a radial contraction (a) (Video 20, left). Closer to the rings forming the embryo prepattern, the oscillations are anisotropic and oriented along the ring pattern (b) (Video 20, right). When the deformation of the presumptive territory of the amniotic sac is followed by PIV it is observed that the ring of cells constricts progressively but with multiple twitches of contraction [(c), from Video 3, data obtained by following the position of two points in the belt of aligned cells]. Similar oscillations are observed in the crocodile and the chicken embryo amniotic sac. Similar oscillations or contraction spikes are observed ventrally also in the extraembryonic tissue.

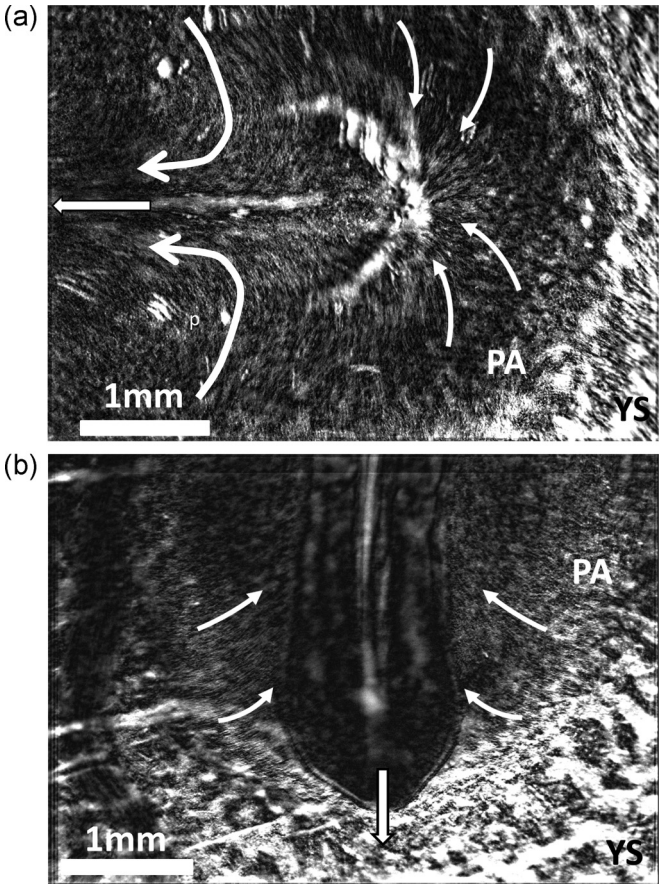

FIG. 19. Streamline patterns during ventral contraction. On average, the contraction is centripetal and folds the embryo ventrally. (a) Anterior area; (b) posterior area. Each of these contractions generates a ventral ring which constricts like a purse string until closure around the navel ([20]).

20(d), Video 25 [25]). Nonlinear contractions, both focal and anisotropic, were also observed ventrally on embryos incubated upside down (Video 26 [25]).

F. Crocodile embryos

In crocodile we found, as in chicken, the existence of a circular ring of cells forming the presumptive amniotic sac territory (Fig. 21, left). Although the study in the reptilian model was not as detailed as in chicken [due to the complexity of crocodile egg dissection at such early stages; see the Appendix: Materials and Methods], we observed that the amniotic sac starts off by a fold in the anterior area, which progresses down the median axis by the purse-string effect. This shows that the chicken experiments and observations are representative of an ancestral phenomenon of amnion morphogenesis. The embryo was smaller and denser, but the topology in the anterior area was identical.

However, a simple but striking difference was observed. In the crocodile embryo, the amniotic fold closes down towards the posterior area, while the tail bud is still forming, but does not hang over the average plane of the blastula (Fig. 21, left). Hence, there is no triggering event in the posterior part, able to start the folding process in the tail region. As a consequence, the "string of the purse" forms a loop which is pulled down in the posterior direction by a chronic contraction in its anterior part only. The anterior fold descends all the way down to the posterior area and closes up there, while in chicken, the amnion closes up roughly in front of the navel area of the embryo by two folds triggered at opposite locations across the embryo, and constricting towards each other [Fig. 5(b)].

We were able to generate an image of tissue trajectories during amnion closure for the crocodile amnion [Fig. 11(b)], showing the radial movement exerted by the closing ring. In crocodile the cell alignments could be observed directly under optical microscopy as the cells are larger than in chicken.

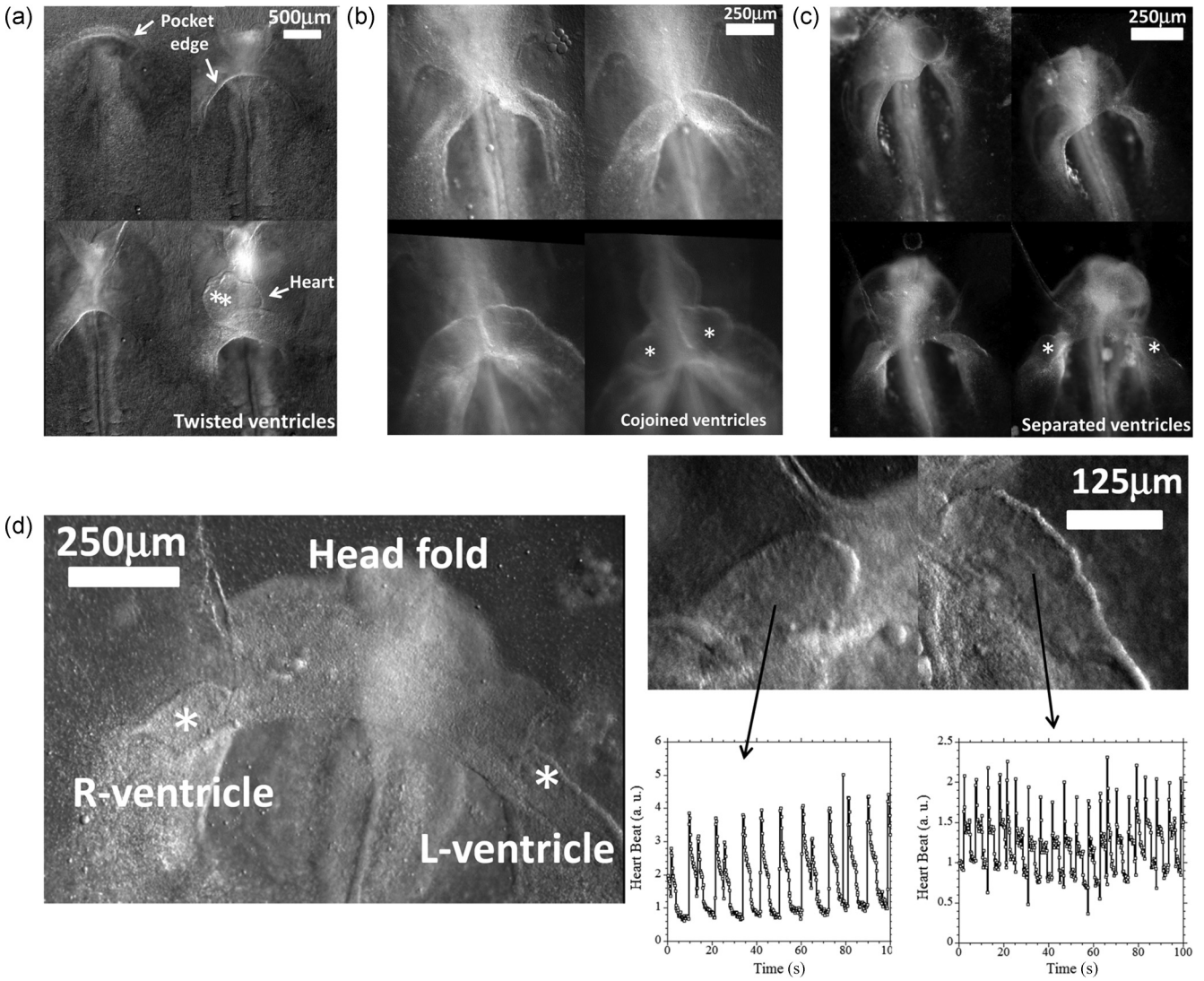

FIG. 20. Normal heart formation, and effect of wounding the ventral purse string. (a) Physiological heart formation (Video 21). The two cardiac territories come together and merge under the effect of the contractile force at the edge of the gut. The left and right ventricles bend, come together, and twist towards the right side. (b) When the edge of the gut is cut (Video 22) at a late stage (>6 somites), the regenerated edge pulls the cardiac territories together (Video 23, duration 10 h). The cardiac ventricles do not, however, twist as observed in the physiological case. (c) When the edge of the gut is cut early (<6 somites), the regenerated edge creeps, and two separated cardiac ventricles form (Video 24, duration 10 h). (d) Observation of the beat of the separated ventricles. When the edge of the gut ring creeps laterally, and two well separated ventricles are formed, each ventricle beats at its own pace (see Video 26). In this plate and in Video 26, the two ventricles are imaged separately, and a combined video and plate is generated showing the two ventricles which are actually far apart (∼1 mm).

Streams of cells clearly following the stretch pattern could be observed on the amnion [Fig. 13(c)].

We observed with consistency (four embryos) that the tail would eventually hang outside the amniotic bag until the end of amnion closure (Fig. 21, right), and would only be inserted inside the sac by the very end of amnion closure (Video 27 [25]). The crocodile data show that the amniotic ring can be stimulated at one or several spots, and that the position where the amnion fold starts or closes is irrelevant, because the dynamics is quite versatile and the cells are plastic enough to follow the physical cues. We observed very similar twitches of contraction in crocodile, as in chicken, with, however, a larger amplitude (Video 28 [25]).

IV. DISCUSSION AND CONCLUSION

In summary, we have shown that the formation of amniotes follows a sequence of events corresponding to a succession of contractions of encased rings. In the first subsection of the Results (Sec. III A) we have shown that the amniotic ring corresponds to a territory with sharp boundaries between adjacent rings of cells; in Sec. III B, we have shown that the rings have different elastic properties. In Sec. III C, we have shown that cells align along the stiffer area, and that buckling occurs at the boundary of these aligned cells. In Sec. III D we have shown that the aligned cells generate a localized tension, which has morphogenetic and regenerative capabilities. We have also shown that the spatial pattern of tension follows the

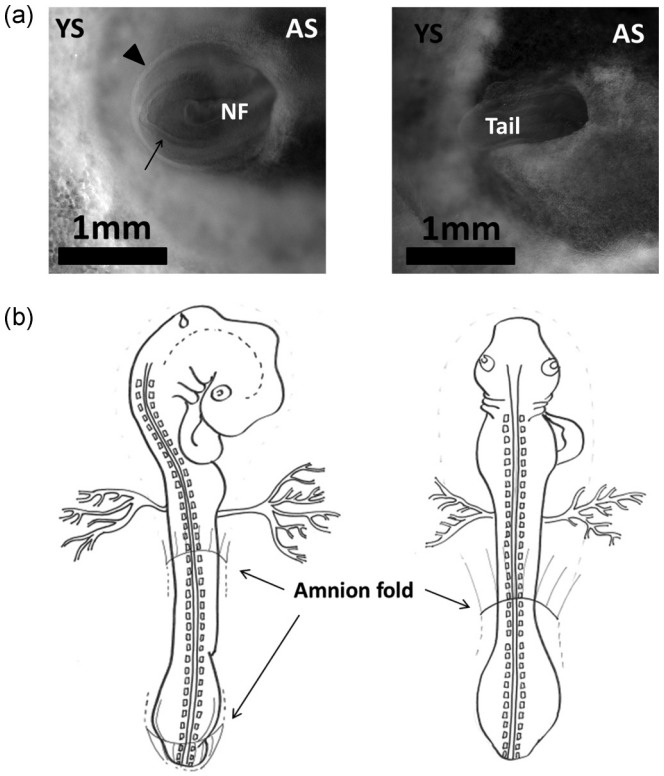

FIG. 21. Crocodile embryo. (a) Left: Image of a crocodile amniotic fold contracting towards the posterior area. The neural fold (NF) in the posterior area is visible, while the tail bud is starting to form (arrow). The presumptive tail is surrounded by a clear circular boundary (arrowhead). In crocodile, the amniotic sac forms by contraction of a wave which wraps the embryo starting from the anterior side only, and propagating all the way down to the posterior part. There is no contraction wave triggered at the posterior side. It is observed that the territory of the blastula is patterned with encased circular rings. The amniotic sac is formed by a fold which follows one ring. (a) Right: Image of amniotic sac closure at a later stage; the tail of the crocodile embryo is found hanging outside the amniotic sac through the opening of the amniotic sac. The insertion into the sac is completed only by the very end of amnion closure (see Video 27). YS = yolk sac; AS = amniotic sac. (b) In chicken (left) the thin territory surrounding the embryo (pellucid area) buckles twice, in the anterior and the posterior regions, and the two folds progress towards each other. In crocodile (right), the pellucid area buckles in the anterior region only and the fold progresses in the posterior direction only, until it wraps the embryo.

ring patterns, and that the contraction is not monotonic. In Sec. III E we have shown that similar features are found for the formation of the ventral folds of the embryo. Finally, we have shown similar results for the crocodile amniotic sac. This work supports the view that there exists a general mechanism at play during amniote morphogenesis. The amniote blastula has a very simple Russian-doll-type structure with cell rings encased in one another. Each ring has a characteristic cell type, cell size, and elasticity. The differences in elasticity between the different rings carry morphogenetic information, as they determine the spatial pattern of force and the position of the embryo folds, and, as shown here, even of the amniotic fold.

We have additionally found that the discontinuity of mechanical properties localizing the amniotic fold is associated with a discontinuity of deformation: Cells at the boundary are sheared orthoradially; they flatten and align against the stiffer side of the boundary. Cells located along the line of elastic property discontinuity behave (Video 10 [25]) as if they were on an edge (of a Petri dish, for example); the discontinuity orients the cells and focuses the tensile force, which is anisotropic along boundaries of cellular territories. This force is exerted via actin cables [21,22] along the domain boundary. Several investigators have reported that mechanical force (tensile in particular) orients cells and their movement in early vertebrate embryos [26–28].

We have shown that the force exerted by the cells is not monotonic. There exist twitches of contraction and relaxation in the presumptive territory of the amnion, at a very early stage (day 2–3 in chicken). These are anisotropic along the cell boundaries forming the rings, and they induce centripetal contractions. We have also shown that the amniotic fold is certainly triggered by the tail bud in chicken, in the posterior area.

We also observed the embryo upside down by time lapse, which clearly revealed that the gut pocket pulls on the anterior area where the amniotic sac first folds. This area was also observed in SEM which confirms the physical connection between the gut fold and the amniotic fold (Fig. 22). It is therefore likely that the heart and gut folds actually trigger the formation of the amniotic sac in the anterior area. In crocodile, the amniotic fold is not triggered in the posterior area. This remarkable difference between chicken and crocodile amnions reminds one of the experimental assay reported by Adamstone in Ref. [29]. Indeed, in chicken, if the presumptive territory of the posterior fold of the amnion is burned by some microsurgical intervention as in Ref. [29], it is observed that the anterior fold will continue the closure process, until it reaches the chicken's tail, and will close around the posterior area, instead of doing so around the mid-dorsal area. This shows that the crocodile situation is just a remarkable ancestral instance of this microsurgical assay.

The effect of gut pocket wounding on heart morphogenesis extends results obtained by Voronov and Taber [30]. These authors suggested that bending of the ventricles is intrinsic to the ventricles rather than an effect of the contractile force that brings them in contact with one another. Our observations lend support to this notion, as we observed that bending of the right ventricle occurred even though the two ventricles did not merge properly (Video 23, ventral view; the right ventricle is to the left). The fate of each ventricle is thus predetermined and does not require contact of the two ventricles. These wounding experiments show that the process of contraction of the rings has far reaching morphological consequences, and it does not solely contribute to formation of purse strings closing the embryo folds.

The sporadic focal contractions and relaxation twitches, together with the induction of the posterior fold by the tail, demonstrate that the amniotic contractions are excitable. It is classical in physiological studies of myogenic contractions that the amplitude and the period of the contraction may increase up to a tetanic phase corresponding to a permanent plateau contraction [31]. This is especially the case when the stimuli

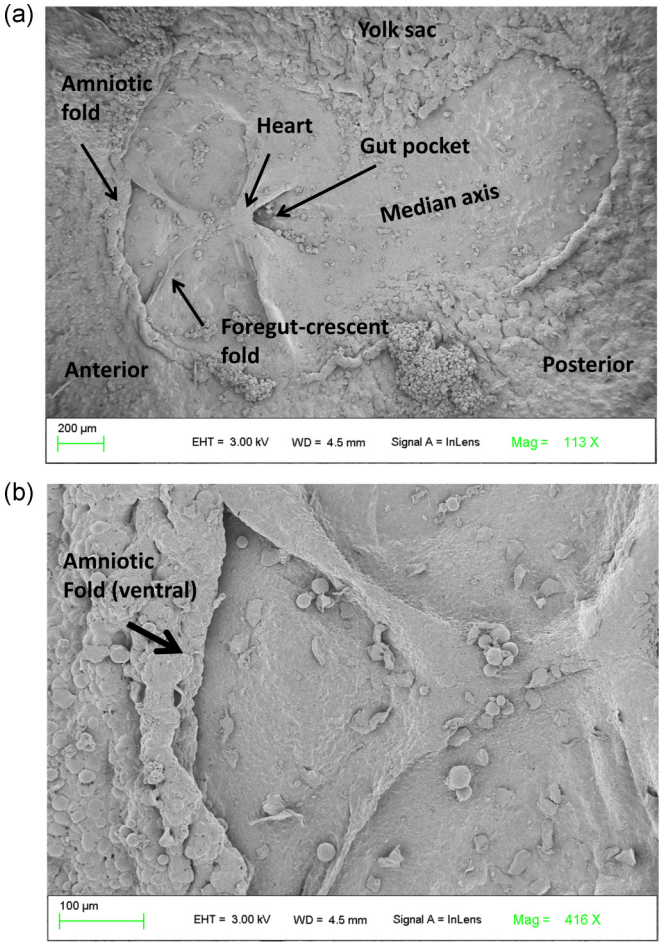

FIG. 22. SEM ventral views of the embryo showing the folds along the edge of the gut crescent. These folds are pulled posteriorly by the ventral purse string and heart, and they pull on the anterior area, thus triggering the amniotic fold.

propagate from one pacemaker to another in time scales shorter than the relaxation time, such that contractions sum up. The observation of intermittent anisotropic twitches, having the same spatial pattern as the contraction generating the folds, suggests that the morphogenetic contractions in the embryo are the tetanic limit of the observed twitches. The ring structure would favor the coupling between pacemakers by rendering pulse propagation more one dimensional.

These observations also suggest that each event sets off the following one: the rotatory movements along the initial ring generate tissue involution and a posterior pull [4]; the posterior pull generates the neural folds and triggers the ventral contraction. Finally the ventral contraction, by stressing the next ring, triggers amnion formation. It does not matter for amnion formation whether the tissue is excited twice, anteriorly and posteriorly, as in chicken, or only once as in crocodile, since the final shape of the pattern is locked to the rings' geometry.

This seems to provide a straightforward explanation of the chronological order in which the folds form in vertebrate embryos, each ring contraction inducing the next one.

We have also shown that after cutting the amnion, cells located close to the edge realign *in vivo* quickly under the effect of the tensile force. Any cell located in the thin pellucid area can contribute to the purse string. The cells that surround the ridge of the amnion deeper within the pellucid area align perpendicularly to the ridge. In both cases, cell orientation is plastic and sensitive to the local stress. We found that the physiological time constant for cell alignment due to tension in the amniotic belt is about 10 min. This value is consistent with other reports on puncturing of closed amnions [22]. *In vivo* imaging in crocodile shows that this cellular plasticity is ancestral.

Cell alignments at the boundary between different physiological compartments (rings in the Russian-doll structure of the blastodisk) are also observed at the boundary between the lateral plate of the blastoderm and the pellucid area (Fig. 23). These cell alignments along textural boundaries (rings) ensure the consistency of morphogenesis as they provide the anisotropy of the contractions and enable the physical separation by buckling of regions of different cell type. Anisotropic contractions certainly contribute to self-organization of the embryonic texture, since the time constant of the contractions is in the same range as the time constant of cell reorientation ($\sim$5 min for relaxation of contractions, $\sim$10 min for cell reorientation). It is observed that the contraction events generating the folds are preceded by a slow phase during which alignment is enhanced until nonlinear buckling occurs.

The experiments reported here show that tensile force as well as tensile-force sensing play both a morphogenetic self-organization role and a regenerative role. This seems to be a general feature of embryonic regeneration [28]. The simple experiments on a rubber sheet illustrate the simplicity of the physical principles at play (Fig. 17).

One may wonder how evolution should have succeeded in evolving amniotes. Since a characteristic of cell division with differentiation is to generate cells with different morphologies [32,33], the boundaries between differentiated stripes exhibit *de facto* a mechanical contrast. This makes folding at differentiation lines likely, since structural defects such as ribs of "stiffeners" are well known in thin plate technology to highly localize buckling on the softer side of the rib [34]. However, stiffening may also come from thickening. We did not address the question of how the mesoderm is spread under the surface of the embryo (the ectoderm), and how it contributes to stiffening of the different areas. Stiffening may also be directly linked to cell alignment, since aligned cells are more densely packed in the transverse than in the longitudinal direction. This would explain the localization of the amniotic fold at the very edge of the belt of aligned cells. It is classical in liquid-crystalline elastomer science that phase transitions with orientation as order parameter is associated to critical changes in elastic parameters [35], in a similar way as viscosity of liquid crystals depends on the ordering of the phase.

Oscillations similar to the ones reported here have been reported at later stages of development [36]. A question for future studies is whether these oscillations are related to early peristalsis in embryonic tubes (lung, gut, etc.). Smooth muscle oscillations are observed quite early in embryonic development. Such peristaltic oscillations in the lung or the gut are known to start off weak and disorganized, and to progressively become stronger and more directional [37]. It would make sense that even the phase of weak and

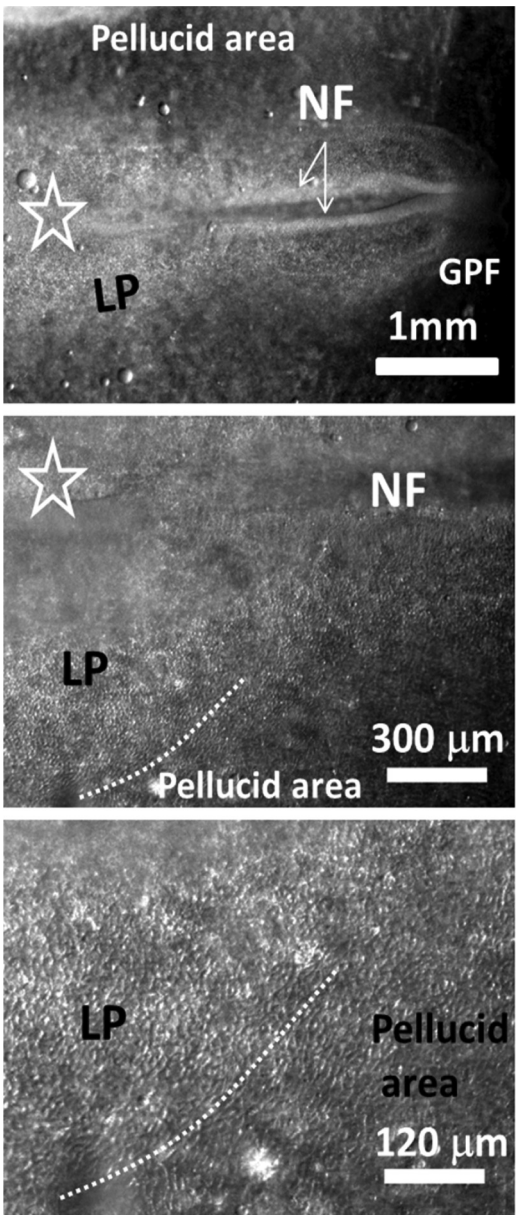

FIG. 23. Generality of cell alignments. Cell alignments are also observed at the boundary between the lateral plate of the embryo and the pellucid area, where there is also a discontinuity in elastic properties. The photographs show a zoom into the cell organization along the lateral plate of a neurulating embryo. The neural folds are just appearing. There is a boundary between two domains characterized by different cell sizes. At the boundary between the two domains, cells align in a pattern that simply follows the boundary as it is deformed in the viscoelastic tissue flow. The star shows the position of Hensen's node. The dashed line signals the orientation of cells. To the right are the early neurulation folds forming the presumptive head. LP: lateral plate; GPF: gut pocket fold; NF: neural fold.

disorganized contractions in the lung, gut, or kidney ducts would be preceded by an even more disorganized phase occurring sporadically on the "flat" embryo (the blastoderm), prior to rolling up of the tissues into the form of tubes. In this respect, the ridge of the purse string would correspond to the transition between a flat tissue and a tubular tissue, thus exhibiting already more organized contractions along the forming ring.

ACKNOWLEDGMENTS

We thank the Laboratoire d'Excellence "Who Am I" for giving the fertilized chicken eggs for this study. We thank Jean-Loup Duband for his interest in this work and stimulating discussions. We thank the reptilarium Alligator Bay for providing the crocodile embryos free of charge. We thank the high school students of the Collège Thomas Mann, Zakaria Benreguig and Zoe Fulchiron, for providing the photos for Fig. 16, during an internship in our laboratory. The IMAGEJ software is courtesy of Wayne Rasband (NIH). We thank O. Cardoso and B. Abou (Lab. MSC) for providing the PIV plug-in. We thank Ludovic Mouton from the ITODYS laboratory, for his kind help with the SEM.

Ethics Statement. The experiments were conducted under French law article R214-87 modified by the Décret No. 2013-118 to comply with European Union regulations. For chicken or crocodile embryos sacrificed during the first third of development, the approval by an ethics committee is not required as for fundamental research.

APPENDIX: MATERIALS AND METHODS

All chicken embryos were purchased at EARL Les bruyères 3, rue du moulin 28190, Dangers, Eure-et-Loir, France. Prior to opening the eggs, and transferring the embryos for experiments, the eggs were incubated in standard incubators (Memmert).

1. Amnion time lapse

Amnion time lapse was performed in the following way. The egg shell is broken and the content of the egg is transferred carefully to a plastic cup. The embryo is always at the top because of buoyancy. The vitelline membrane is cut circularly at a radius of ∼2 cm, around the embryo. The embryo+the vitelline membrane+the vitelline gel are transferred to a Petri dish. Next, the excess of yolk remaining on the embryo is carefully removed by slowly rinsing the sample. Next the embryo+vitelline membrane+gel are transferred to a large (8-cm) glass disk with a spoon. Next a circle of albumin is deposited around the embryo at ∼4 cm. Next a Minitüb thermoregulator with a round window is deposited on the glass disk, the albumin serving as glue. The glass disk+Minitüb incubator with the sample inside is transferred to a Nikon Eclipse microscope having objectives 4×, 10×, and 20× with long working distance able to accommodate the thickness of the Minitüb thermoregulator (8 mm). At this early developmental stage, the weight of the mass of gel suffices to stretch the embryo; however, the embryos can also be stretched on their substrate. All videos were acquired with a monochrome HD camera, Stingray 200, from Allied Vision Technologies interfaced with SMARTVIEW and processed with IMAGEJ (courtesy of Wayne Rasband, NIH). The movements of the embryo and of the dynamometers were analyzed using the particle imaging velocity (PIV) method, with the TRACKER module in IMAGEJ (courtesy of Olivier Cardoso and Bérangère Abou). The image analysis modules are freely available upon request.

2. Shadowgraph imaging

Shadowgraph imaging was performed in the following way. A custom copper window was made, with two slits (width 6 mm), one for the observation of the embryos, one for passing the illumination. The light is produced by a Schott lamp, 2500 W, with a dichroic reflector, which has a small aperture angle ($\sim 15^{\circ}$). The light is guided by a fiber and approached at 45° towards the slit reserved for the light. The light beam is oriented towards the edge of the slit, thus generating by diffraction a thin light sheet of near parallel light used for the shadowgraphic illumination. The two-slit device is displaced until the observation slit is close to the field of view, cutting off diffused light, and letting mostly the shadowgraphic light pass. This enhances surface details by diffraction and reflection of the reflected light on the sample-medium interface, and it allows one to form rapidly, at almost no cost, cell-resolved images of the surface of the embryo. These images are of a good enough quality to image cell sizes and orientations; however, as the shadowgraphic contrast is not uniform (it depends on surface topography), it does not allow an automated segmentation of cell membranes.

3. Glass cantilever tractions on the amnion

The measurements with the glass cantilever were done following the method described in Ref. [38] for studies of embryonic gut mechanics, but adapted to the amnion case. To summarize, a long and thin glass pipette is pulled manually. Its very end is bent in the form of a hook. The pipette is attached to a motorized translational stage (Newport), piloted by a macro in NIH IMAGE software. The embryo is removed from the egg, detached from the vitelline membrane, and transferred to a square box filled with PBS. The bottom is covered with black rubber foam (RS 733-6757). The embryo is carefully deposited on the bottom, and stretched on the foam. The square box is observed laterally with an Optem zoom (Thomson) at magnification $1\times$ to record the deflection of the cantilever. Simultaneously, the embryo is observed from atop with a similar optics. Two Stingray monochrome cameras interfaced with AVT SMARTVIEW software from Allied Vision Technologies were used to film the cantilever and the samples. A rather high level of PBS (~ 3 cm) is poured into the square box to avoid meniscus offset effects during bending of the cantilever. The cantilever used was calibrated by hanging small weights on the terminal hook, which were cut from a polypropylene thin thread. The calibration of the cantilever showed a linear elastic response of the cantilever with a flexion stiffness of $2 \times 10^{-2}\,\mathrm{N\,rad^{-1}}$, i.e., $3.5 \times 10^{-4}\,\mathrm{N/deg}$.

4. Scanning electron microscopy

The embryos at stage 15 (Hamilton Hamburger stages—when the limb primordia first appear) are fixed using 4% paraformaldehyde in PBS. They are immersed in the fixative for 15 min and then rinsed with distilled water three times. After being fixated they are immediately dried by the supercritical drying method in a Bal-tec CPD 030 critical point dryer. For the process of critical drying the embryos are placed on square glass slides of length 1.5 cm. They are then stacked in a square glass container which is finally wrapped in filter paper. The free ends of the paper are tied together to form an enclosed parcel. This ensures that the embryos remain surrounded by fluid throughout the process until they reach critical point. The parcel is then immersed in a solution of 50% ethanol. The concentration of ethanol is serially increased by removing half of the volume of solution in the chamber and replacing it with an increasing concentration of ethanol solution. When the entire solution is replaced with 100% ethanol the package is placed in the critical drying chamber. The ethanol medium is then replaced in a serial manner with liquid carbon dioxide. A magnetic stirrer is used to facilitate uniform mixing of the solution. This is continued until the chamber is filled with 100% liquid CO_2. After medium exchange the chamber is heated up to 40 °C. The pressure in the chamber increases with increase in temperature. At 40 °C and 100 bars pressure the entire chamber is filled with gaseous CO_2. The pressure is then released slowly, using the metering valve, to avoid condensation. The samples are then metallized where they are coated with gold. The metallized samples are viewed under the Zeiss Supra 55VP field emission scanning electron microscope. Different regions of the tail end are studied in increasing magnification.

5. Crocodile eggs preparation

The eggs of the Nile crocodile *Crocodylus niloticus* were obtained from Alligator Bay, Mont St Michel, in Normandy, France. They were stored in a refrigerator at 14 °C before experimentation. In the lab they were incubated at 32 °C to have a faster growth rate. Crocodiles are known to exhibit temperature dependent sex determination; that is, the sex of the embryo depends on the temperature of their incubation. Males are born when eggs are incubated at temperatures between 18 °C–31 °C and above or below this temperature female offspring are observed. Two- to five-day-old eggs are dissected to study the growth and development of the embryo.

The eggs are washed thoroughly to remove mud and urine from the surface. Care is taken not to rock the eggs as the vitelline membrane tends to get attached to the inner shell membrane after days of immobile incubation and excessive movement during this period causes traumatic tearing of the embryo. The shell is then removed piece by piece to expose the outer surface of the shell membrane. The shell membrane is multilayered and fibrous in texture. After the shell is completely removed the egg is placed in a glass Petri dish. The egg retains its shape because of the thick shell membranes. The membrane is cut with scissors in a circular manner perpendicularly to the long axis of the egg. The contents of the egg are gently emptied into the Petri dish. A gelatinous thick albumin layer is seen on top of the yolk and less viscous thin albumin flows to the sides of the thick albumin and yolk. Excess of albumin is cut in piecemeal fashion and removed with forceps to prevent the loss of embryo in the thick gelatinous mass. The yolk is pale yellow in color and more viscous and homogeneous than the darker, globular yolk seen in chickens. The vitelline membrane is a thin delicate layer between the yolk and the albumin. It tends to break or tear spontaneously when the egg is placed in the Petri dish due to the stretching and flattening of the yolk. For ease of dissection some of the yolk is sucked out using a wide-bore

needle from the side opposite to the embryo. This prevents the rapid outflow of yolk along with the embryo bearing vitelline membrane.

After the embryo is isolated it is washed gently with phosphate buffered saline to remove the yolk droplets. It is then transferred with its dorsal side facing upwards on a preprepared substrate of chicken thick albumin and vitelline membrane. It is filmed under a light microscope for time-lapse studies and particle image velocimetry. It must be noted that vitelline membrane shrinks drastically as soon as it is cut or torn. This results in the folding of the more fragile young embryos before the physiological folding. This is why embryos at the blastula stage could hardly be recovered by this procedure. Only one embryo at the primitive streak was recovered. On average the procedure is much more difficult than for chicken embryos. In addition, since all eggs are laid in a single clutch of 20–30 eggs, the actual developmental time of the eggs is spread by 0 to about 3 days. As a consequence about 100 eggs were opened, out of which only about 40 were fertilized, and only about 10 were exploitable in the developmental window of this study.

6. Miscellaneous observations (Crocodiles)

The albumin has radiating folds in the surface that is in contact with the vitelline membrane. In some of the eggs the albumin layers have a uniform greenish discoloration. This is observed more often in fertilized eggs. The amniotic sac appears thicker than in chicken with a prominent medial raphe. Most of the embryos that were dissected had completed amniotic folding or enclosing of the head region, except one for which the contraction and folding of the cellular ring forming the amnion could be observed by time lapse *in vivo*. The crocodile embryos appear to be bilaterally symmetrical in development. The structure of the heart, as observed ventrally by turning the embryos upside down, is simpler and tubelike. The head does not rotate to the right as seen in chicken.

7. Elastomer cantilever tractions on the pellucid area

The elasticity of the pellucid area was measured by in-plane traction with a small piece of filter paper attached to an elastomer cantilever. The paper used to pull or compress the embryos had the same width as the pellucid area. The elastomer cantilever is a thin CAF4 (Rhodorsil) thread made by spreading CAF4 on a Teflon plate as described in Ref. [4]. Here, instead of using the CAF4 thread as a traction dynamometer, as in Ref. [4], we use it as a flexion dynamometer (higher precision). A small piece of filter paper is glued at the tip of the CAF4 cantilever. The embryo is descended in a square box as described previously. The filter paper approaches the yolk sac, as close as possible to the pellucid area. The paper is gently pressed on the yolk sac. It adheres sufficiently for traction measurement. We assume that the fibers of the filter paper get entangled in the yolk sac surface and villosities. Next the tool is moved by an automated translation stage, as described above. The flexion of the elastomer is measured optically by PIV. The elastomer cantilever is calibrated by flexing it with the glass cantilever described above, used as a proxy. The calibration of the cantilever showed a stiffness of the order of 1.5×10^{-4} N/mm flexure. A deformation of 10% of the pellucid area is found for $\sim 12\ \mu$N. An offset is found for small forces likely due to embryo friction on the substrate (Fig. 24).

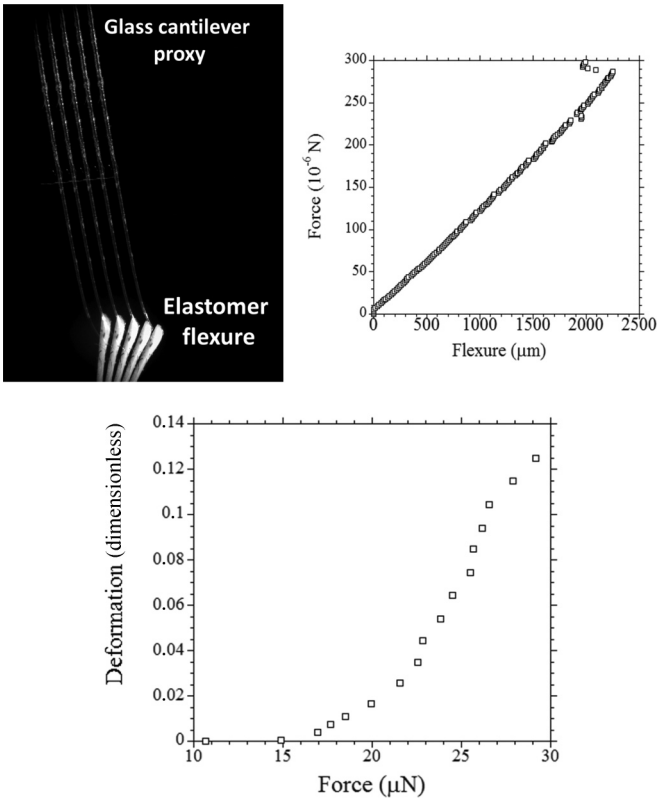

FIG. 24. Top: Calibration of the elastomer cantilever, with the glass cantilever used as a proxy. The elastomer is calibrated by flexing it with the glass cantilever of known stiffness. Bottom: Typical force measurement in an embryo traction experiment performed with an elastomer dynamometer. In the embryo stretch experiment, the deflection of the elastomer cantilever is followed with a camera by PIV. This gives the applied force. The average tissue deformation of the embryo is then plotted as a function of the applied force. Actually, the absolute value of the force is not crucial for proving the existence of a stiffness contrast. Experiments show that the deformation in the tissue is actually much less noisy than the force measurement; therefore, the ratio of deformability in the embryo gives a fair measurement of stiffness contrast.

[1] V. Fleury, Organogenesis **2**, 6 (2005).
[2] C. Cui, X. Yang, M. Chuai, J. A. Glazier, and C. J. Weijer, Dev. Biol. **284**, 37 (2005).
[3] V. Fleury, BioSystems **109**, 460 (2012).
[4] V. Fleury, N. Chevalier, F. Furfaro, and J.-L. Duband, Eur. Phys. J. E **38**, 1 (2015).
[5] E. Rozbicki, M. Chuai, A. Karjalainen, F. Song, H. M. Sang, R. Martin, H.-J. Knölker, M. P. MacDonald, and C. J. Weijer, Nat. Cell Biol. **17**, 397 (2015).
[6] T. Savin, N. A. Kurpios, A. E. Shyer, P. Florescu, H. Liang, L. Mahadevan, and C. J. Tabin, Nature **476**, 57 (2011).
[7] M. Küecken and A. C. Newell, J. Theor. Biol. **235**, 71 (2005).

[8] S. Gilbert, *Developmental Biology* (Sinauer Press, Sunderland, MA, 1996).
[9] V. D. Varner, D. A. Voronov, and L. A. Taber, Development **137**, 3801 (2010).
[10] X. Chen and G. W. Brodland, Phys. Biol. **5**, 015003 (2008).
[11] A. L. Romanoff, *The Avian Embryo: Structural and Functional Development* (Macmillan, London, 1960).
[12] R. Bellairs and M. Osmond, *Atlas of Chicken Development* (Academic Press, Cambridge, MA, 2014).
[13] P. O. Favaron, R. C. Carvalho, J. Borghesi, A. Anunciaçao, and M. A. Miglino, Reprod. Domest. Anim. **50**, 881 (2015).
[14] V. Hamburger and H. L. Hamilton, Dev. Dyn. **195**, 231 (1992).
[15] C. Darwin, *On the Origin of Species by the Means of Natural Selection* (John Murray, London, 1859).
[16] R. Owen, *On the Nature of Limbs. A Discourse* (John Van Voorst, London, 1848).
[17] N. Brocklehurst, M. Ruta, J. Müller, and J. Föbisch, Sci. Rep. **5**, 17104 (2015).
[18] R. R. Reisz, Trends Ecol. Evol. **12**, 218 (1997).
[19] F. Davidson, A descriptive and experimental study of amniotic fold formation in the chick embryo, Ph.D. dissertation, The University of Texas at Austin, 1977.
[20] V. Fleury, C. R. Acad. Sci. Biol. **334**, 91 (2011).
[21] N. Tipping and D. Wilson, Anat. Rec. (Hoboken) **294**, 1143 (2011).
[22] C. F. MacManus, N. E. Tipping, and D. J. Wilson, Wound Repair Regener. **14**, 61 (2004).
[23] M. C. Milinkovitch, L. Manukyan, A. Debry, N. Di-Poï, S. Martin, D. Singh, D. Lambert, and M. Zwicker, Science **339**, 78 (2013).
[24] O. Weeks, B. Bhullar, and A. Abzhanov, Evol. Dev. **15**, 393 (2013).
[25] See Supplemental Material at http://link.aps.org/supplemental/10.1103/PhysRevE.94.022426 for videos of embryo development and experimental assays during amnion formation.
[26] R. L. de Haan, Exp. Cell. Res. **29**, 544 (1963).
[27] N. Nakatsuji and K. E. Johnson, Nature **307**, 453 (1984).
[28] M. Nodder and P. Martin, Anat. Embryol. (Berlin) **195**, 215 (1997).
[29] F. B. Adamstone, J. Morphol. **83**, 359 (1948).
[30] D. A. Voronov and L. A. Taber, Dev. Dyn. **224**, 413 (2002).
[31] J. D. Aidley, *The Physiology of Excitable Cells*, 4th ed. (Cambridge University Press, New York, 1998).
[32] A. Cicalese, G. Bonizzi, C. E. Pasi, M. Faretta, S. Ronzoni, B. Giulini, C. Brisken, S. Minucci, P. P. Di Fiore, and P. G. Pelicci, Cell **138**, 1083 (2009).
[33] D. Rudel and R. J. Sommer, Dev. Biol. **264**, 15 (2003).
[34] I. Elishakoff, Y. W. Li, and J. H. Starnes, Jr., Chaos, Solitons Fractals **5**, 1517 (1995).
[35] E. M. Terentjev, J. Phys.: Condens. Matter **11**, R239 (1999).
[36] M. V. Nechaeva and T. M. Turpaev, Comp. Biochem. Physiol., Part A: Mol. Integr. Physiol. **131**, 861 (2002).
[37] K. K. Bokka, E. C. Jesudason, O. A. Lozoya, F. Guilak, D. Warburton, and S. R. Lubkin, PLoS One **10**, e0132015 (2015).
[38] N. Chevalier, E. Gazquez, S. Dufour, and V. Fleury, Methods **94**, 120 (2016).